

Water vapor emission from IRC+10216 and other carbon-rich stars: model predictions and prospects for multitransition observations

Eduardo González-Alfonso

*Universidad de Alcalá de Henares, Departamento de Física, Campus Universitario,
E-28871 Alcalá de Henares, Madrid, Spain*

eduardo.gonzalez@uah.es

David A. Neufeld

*Department of Physics & Astronomy, The Johns Hopkins University, 3400 N. Charles
Street, Baltimore, Maryland 21218*

and

Gary J. Melnick

Harvard-Smithsonian Center for Astrophysics, 60 Garden Street, Cambridge, MA 02138

ABSTRACT

We have modeled the emission of H₂O rotational lines from the extreme C-rich star IRC+10216. Our treatment of the excitation of H₂O emissions takes into account the excitation of H₂O both through collisions, and through the pumping of the ν_2 and ν_3 vibrational states by dust emission and subsequent decay to the ground state. Regardless of the spatial distribution of the water molecules, the H₂O $1_{10} - 1_{01}$ line at 557 GHz observed by the *Submillimeter Wave Astronomy Satellite* (SWAS) is found to be pumped primarily through the absorption of dust-emitted photons at 6 μm in the ν_2 band. As noted by previous authors, the inclusion of radiative pumping lowers the ortho-H₂O abundance required to account for the 557 GHz emission, which is found to be $(0.5-1) \times 10^{-7}$ if the presence of H₂O is a consequence of vaporization of orbiting comets or Fischer-Tropsch catalysis. Predictions for other submillimeter H₂O lines that can be observed by the *Herschel Space Observatory* (HSO) are reported. Multitransition HSO observations promise to reveal the spatial distribution of the circumstellar water vapor, discriminating among the several hypotheses that have been proposed for the origin of the H₂O vapor in the envelope of IRC+10216. We also show that, for observations with HSO, the H₂O $1_{10} - 1_{01}$ 557 GHz line affords the greatest sensitivity in searching for H₂O in other C-rich AGB stars.

Subject headings: Stars: abundances — Stars: AGB and post-AGB — stars: individual (IRC+10216) — ISM: molecules — radiative transfer — submillimeter

1. Introduction

The discovery of water vapor emission in the extreme C-rich AGB star IRC+10216 with SWAS (Melnick et al. 2001), its confirmation by ODIN (Hasegawa et al. 2006), and the subsequent detection of other O-bearing molecules like OH (Ford et al. 2003), H₂CO (Ford et al. 2004), and C₃O (Tenenbaum et al. 2006), have challenged our current understanding of the chemistry in envelopes around C-rich AGB stars. According to standard models, essentially all oxygen nuclei are predicted to be locked into CO or SiO with no reservoir to form other O-bearing molecules (except for low abundances of species such as HCO⁺ in the outer envelope where photochemistry is important). Therefore, the unexpectedly high abundances found for H₂O, OH, and H₂CO, indicate that several processes not included in standard models for C-rich environments are driving the oxygen chemistry, but the dominant water production mechanism is still a source of debate.

Four distinct mechanisms have been considered as possible sources of the observed water vapor in IRC+10216, each one making a specific prediction for the H₂O spatial distribution in the envelope: (*i*) chemistry in the inner envelope, which would imply the presence of H₂O in the warmest and densest regions; (*ii*) vaporization of icy orbiting bodies that have survived from the main sequence into the C-rich AGB phase (Melnick et al. 2001; Ford & Neufeld 2001), predicting the release of H₂O at intermediate radii of $R_{int} = (1 - 5) \times 10^{15}$ cm; (*iii*) grain surface reactions, such as the Fischer-Tropsch catalysis on the surfaces of small metallic grains (Willacy 2004), which predicts H₂O to attain a nearly uniform abundance at radii larger than $R_{int} = (1.5 - 2) \times 10^{15}$ cm; (*iv*) chemistry involving photodissociation products in the outermost regions of the envelope: a specific mechanism relying on the radiative association $O + H_2 \rightarrow H_2O + \gamma$ has been proposed by Agúndez & Cernicharo (2006, hereafter AC06), and predicts H₂O to be present at radii higher than $R_{int} \approx 4 \times 10^{16}$ cm. In all cases, H₂O is expected to have a uniform abundance from R_{int} up to the external region where it is photodissociated producing OH.

The only water line detected so far in IRC+10216, the ortho-H₂O $\hat{1}10101$ transition at 557 GHz, is the ground-state transition, with the upper level at only 27 K above the ground rotational level, and cannot discriminate -by itself- between the processes listed above. Nevertheless, the launch of the Herschel Space Observatory (HSO) will allow us to observe other H₂O lines in the submillimeter and far-infrared domains, permitting us to infer the region where the H₂O emission arises, and will potentially favor one of the

proposed formation mechanisms. The Heterodyne Instrument for the Far Infrared (HIFI) onboard HSO will provide very high spectral resolution observations (0.14-1.0 MHz), thus permitting the lines to be velocity resolved. In this paper, we model the H₂O emission from IRC+10216 to show how the H₂O spatial distribution can be inferred from HSO multi-transition observations. Also, we explore which H₂O transition provides the most sensitive means of searching for water vapor around AGB stars other than IRC+10216; such a search would determine whether the occurrence of H₂O in C-rich environments is widespread.

2. Model description

Our model for IRC+10216 assumes a stellar mass loss rate of $\dot{M} = 3 \times 10^{-5} M_{\odot} \text{ yr}^{-1}$. The gas velocity field, turbulent velocity, and H₂ density and gas temperature profiles are those adopted by Melnick et al. (2001) (see references therein), and listed in Table 1. A distance to the source $D = 170$ pc is assumed.

The adopted gas temperature profile is an approximate fit (e.g. Glassgold 1996) to the results obtained by Kwan & Linke (1982), who calculated the thermal profile through the circumstellar envelope of IRC+10216 from the energetic balance between gas heating and cooling. These calculations included gas-dust collisional heating and both adiabatic and CO line cooling. HCN line cooling was ignored and, subsequently, the ISO far-infrared spectrum of IRC+10216 showed strong HCN rotational emission from both the ground and excited vibrational states (Cernicharo et al. 1996). Nevertheless, radiative transfer calculations appear to indicate that HCN radiative excitation through absorption of infrared photons emitted by warm dust dominates over collisional excitation (González-Alfonso & Cernicharo 1999a; Dinh-V-Trung & Nguyen-Q-Rieu 2000), and in such a case the observed HCN emission would not involve any further cooling.

It is shown below that the continuum emission provides the dominant excitation source for all H₂O lines of interest, mainly through absorption of 6 μm photons in the ν_2 band and subsequent decay, and so a model for the dust emission from IRC+10216 is required. We have used a radiative transfer code to compute, from the balance between heating and cooling at any radial position in the envelope, the dust temperature profile (González-Alfonso & Cernicharo 1999b). Our model simulates the dust properties by making use of an empirical spectral index β . The inferred dust parameters are listed in Table 1, and the goodness of the fit, shown in Fig. 1, ensures that the continuum radiation density is well reproduced at least at $r \gtrsim 2 \times 10^{15}$ cm, where it varies as $\sim r^{-2}$.

The radiative transfer code used to determine the H₂O excitation and emission has

been described in González-Alfonso & Cernicharo (1997, 1999b). The calculations assume spherical symmetry, and the envelope is divided into 60 spherical shells to account for the variations in the physical and chemical conditions with distance to the star. The dust and H₂O are assumed to be coexistent within any shell, and the non-local radiative transfer is simulated through rays that cross the source. The code first computes the H₂O statistical equilibrium populations at any radial position in the envelope with the use of an iterative procedure based on an approximate Newton-Raphson operator (Schönberg & Kempe 1986). A maximum relative variation of populations of 10⁻³ was established as the convergence criterion; a much tighter criterion was found in some test models to change line fluxes by at most 0.2%. Once convergence is achieved, the resulting line profiles and fluxes are calculated. We report the expected intensities in units of main-beam temperature (T_{MB}), with a half-power beam width of HPBW=240" to simulate SWAS measurements, and HPBW ranging from 12".5 (1703-1910 GHz) to 41" (480-640 GHz) for HSO-HIFI observations (see Table 3, below).

Spectroscopic data for H₂O were taken from the Hitran 2004 database (Rothman et al. 2005). We included the ground and the $\nu_2 = 1$ and $\nu_3 = 1$ excited vibrational states, but the $\nu_3 = 1$ state was found to have a negligible effect on the emission from the ground state lines. The $\nu_1 = 1$ state was ignored because the ν_1 band is much weaker than the ν_3 band, and more excited vibrational levels are also ignorable because they are weakly connected to the ground vibrational state and/or the continuum emission from IRC+10216 weakens in the near infrared. Up to 40 rotational levels per vibrational state for both ortho-H₂O and para-H₂O were taken into account, but the code allows this number to be decreased in external regions with low excitation, with the aim of ensuring and accelerating convergence.

The calculations simulate both collisional excitation among rotational levels of the ground vibrational state, and radiative excitation in all transitions. Vibrational excitation through collisions is neglected. Collisional rates among the 10 lowest rotational levels for $T_k \leq 140$ K are taken from Phillips, Malluendes & Green (1996). We extrapolate these rates to higher T_k by multiplying the excitation rates for $T_k = 140$ K by $\exp\{\Delta E(1/140 - 1/T_k)\}$, where $\Delta E(K) = E_{up} - E_{low}$ is the energy difference between the upper and lower levels. The application of this strategy appears to be justified, since the use of the Phillips et al. (1996) collisional rates at $T_k = 140$ K, together with the quoted extrapolation, yield collisional rates for $T_k = 20 - 120$ K that reproduce the values given by Phillips et al. (1996) within a factor of 1.6. Also, some estimate of the collisional rates among levels not considered by Phillips et al. (1996) is required to simulate the collisional excitation in the innermost regions of the envelope. With this aim, we have found that if the H₂O-He collisional excitation rates for the 10 lowest rotational levels given by Green, Maluendes, & McLean (1993), are multiplied by a global factor of 5, *most* of the H₂O-H₂ $J = 1$ rates given by Phillips et al.

(1996) are reproduced within a factor of 2.5; similarly, *most* of the H₂O–H₂ $J = 0$ rates given by Phillips et al. (1996) are reproduced within the same factor if the Green et al. rates are multiplied by a factor of 1.35, the difference in reduced mass when H₂ is the collision partner rather than He. After applying these corrections to the Green et al. (1993) coefficients, some individual rates are still strongly underestimated, by 1-2 orders of magnitude, relative to the Phillips et al. (1996) values, specially in the case of collisions between para-H₂O 0₀₀ and H₂ $J = 1$ (see discussion in Phillips et al. 1996). Nevertheless, the collisional excitation of a high-energy level in high-density and high-temperature regions is the result of collisional pumping from various other levels, and so individual discrepancies are to some extent diluted. In summary, we have used the Green et al. (1993) excitation rates, multiplied by the factors quoted above, to simulate the collisional excitation among levels not considered in Phillips et al. (1996). The adopted extrapolation does not critically affect results because, as shown below, radiative excitation dominates over collisional excitation in all lines of interest.

We have generated a set of models that differ only in the inner radius of the H₂O shell, R_{int} , and in the H₂O abundance, $X(\text{H}_2\text{O})$. The different values of R_{int} account for different spatial distributions of H₂O in the envelope of IRC+10216, and $X(\text{H}_2\text{O})$ is derived in such a way that the predicted flux of the o-H₂O $\hat{1}10101$ is $\approx 10^{-20}$ W cm⁻² as observed by SWAS (Melnick et al. 2001). The ortho-to-para H₂O abundance ratio is assumed to be 3:1. In all models, we have adopted an external radius of the H₂O shell $R_{out} = 4 \times 10^{17}$ cm, where H₂O is assumed to be photodissociated. This value of R_{out} is similar to that obtained by Willacy (2004) and AC06 through photodissociation models of the external shells of the IRC+10216 circumstellar envelope. The photodissociation radius depends on several parameters and could be significantly lower than the quoted value (Ford et al. 2003; Netzer & Knapp 1987), but test models indicate that line flux ratios for $R_{int} \lesssim 8 \times 10^{15}$ cm vary by less than 20% if R_{out} is decreased to 5×10^{16} cm. For high values of R_{int} , we give in section 4.3 an analytic expression for the expected flux of the o-H₂O $\hat{1}10101$ line as a function of both R_{int} and R_{out} , showing that results are not very sensitive to R_{out} as long as $R_{out}/R_{int} \gg 1$.

We have selected three of those models, called *A*, *B*, and *C*, that correspond to the proposed formation mechanisms described in section 1. The adopted values of R_{int} and the inferred ortho-H₂O abundance, $X(\text{o-H}_2\text{O})$, are listed in Table 2. Model *A* simulates H₂O originating in the innermost regions of the envelope. Model *B* applies to both the cometary hypothesis and the Fischer-Tropsch catalysis mechanism. Vaporization of icy bodies predicts that H₂O is released at a radius of $(1 - 5) \times 10^{15}$ cm, depending on the evolutionary stage of the star after the onset of the TP-AGB phase (Ford & Neufeld 2001). The formation of H₂O due to Fischer-Tropsch catalysis on the surfaces of iron grains predicts that the H₂O abundance attains its maximum value at $(1.5 - 2) \times 10^{15}$ cm (Willacy 2004). Therefore, these two models predict similar H₂O spatial distributions, although the Fischer-Tropsch

mechanism appears to be more restrictive. Model *C* assumes H₂O to be generated as a consequence of photodissociation in the outermost regions of the envelope (AC06).

3. Model results

3.1. The H₂O 1₁₀ – 1₀₁ line in IRC+10216

Figure 2 compares the SWAS 110101 ortho-H₂O continuum-subtracted spectrum (from Melnick et al. 2001) with the line profiles obtained for models *A*, *B*, and *C*, with the SWAS beamsize. All models yield similar line profiles because in all three cases the emission region is small compared to the SWAS 4' beam. The line shapes obtained with the smaller ODIN 2' beam (not shown) are also similar because, even in model *C*, 70% of the emission arises within a spherical shell of diameter 1'.5 (2.3 × 10¹⁷ cm), which is significantly smaller than the ODIN beamsize. The o-H₂O abundance (relative to H₂) required to account for the observed flux, is plotted in Fig. 3 as a function of R_{int} ; it increases slowly for low R_{int} because the innermost regions of the envelope contribute little to the emission at 557 GHz. For $R_{int} = 2 \times 10^{15}$ cm (model *B*), the required ortho-H₂O abundance, $X(\text{o-H}_2\text{O}) = 5.4 \times 10^{-8}$ (Table 2), is one order of magnitude lower than that reported previously by Melnick et al. (2001) and Hasegawa et al. (2006). As first noted by AC06 for the case of high R_{int} , this result is a consequence of the pumping of the $\nu_2 = 1$ vibrational state by dust emission at 6 μm and the subsequent decay to the ground state, which dominates the excitation of H₂O in our models. In the case of the o-H₂O 557 GHz line, the importance of mid-IR pumping can be shown as follows. The radiative path that dominates the pump of the 1₁₀ rotational level is 1₀₁ → ν_2 1₁₀ → 2₂₁ → 1₁₀. The associated pumping rate per molecule in the 1₀₁ level is given by $\Gamma_r = B_{lu} \langle J \rangle \eta_1 \eta_2$, where B_{lu} is the Einstein coefficient for absorption of radiation in the 1₀₁ → ν_2 1₁₀ line, $\langle J \rangle$ is the continuum intensity at 6.2 μm averaged over all angles and integrated over the line profile, η_1 is the fraction of molecules in ν_2 1₁₀ that decay to 2₂₁, and η_2 is the fraction of molecules in 2₂₁ that decay to 1₁₀. Ignoring line opacity effects, and estimating $\langle J \rangle$ as

$$\langle J \rangle = \frac{D^2}{4\pi r^2} F_{6.2\mu\text{m}}, \quad (1)$$

where $F_{6.2\mu\text{m}} = 2.5 \times 10^{-13}$ W cm⁻² μm^{-1} is the observed 6.2 μm continuum flux, and r is the distance from the star, one obtains

$$\Gamma_r \approx \frac{0.02}{r_{15}^2} \text{ s}^{-1}, \quad (2)$$

where $r_{15} = r/(10^{15} \text{ cm})$. The ro-vibrational lines are indeed optically thin in all our models. The 1₀₁ → ν_2 1₁₀ and 1₀₁ → ν_2 2₁₂ have similar opacities; for $R_{int} \gtrsim 2 \times 10^{16}$ cm, essentially

all o-H₂O molecules are in the ground 1₀₁ level (Fig. 4a) and the radial opacities of the quoted lines are given by

$$\begin{aligned} \tau_r &\approx 3 \times 10^{-2} \times \left(\frac{0.65 \text{ km s}^{-1}}{\sigma_v} \right) \times \left(\frac{X(\text{o-H}_2\text{O})}{5 \times 10^{-7}} \right) \\ &\times \left(\frac{R_{out}}{R_{int}} - 1 \right) \times \left(\frac{4 \times 10^{17} \text{ cm}}{R_{out}} \right), \end{aligned} \quad (3)$$

which gives $\tau_r \approx 0.25$ for model *C*. The fraction of o-H₂O molecules in excited energy levels is 20–30% at $r \sim 8 \times 10^{15}$ cm and increases sharply with diminishing r (Fig. 4a); therefore, eq. (3) overestimates the opacities for $R_{int} \lesssim 8 \times 10^{15}$ cm. Our models yield maximum values of $\tau_r = 0.30$ for the case of $R_{int} = 4 \times 10^{15}$ cm. All other ro-vibrational o-H₂O transitions have excited lower levels and hence lower opacities.

On the other hand, the collisional pumping rate from 1₀₁ to 1₁₀ per molecule in the 1₀₁ level is $\Gamma_c = n(\text{H}_2) C_{lu}(T_k)$, where C_{lu} is the collisional rate from the 1₀₁ to the 1₁₀ level, and can be written as

$$\begin{aligned} \Gamma_c &\approx \frac{0.01}{r_{15}^2} \times \left(\frac{C_{lu}(300\text{K})}{2.3 \times 10^{-10} \text{ cm}^3 \text{ s}^{-1}} \right) \\ &\times \exp \left\{ -120 \left(\frac{1}{T_k(r)} - \frac{1}{300} \right) \right\} \text{ s}^{-1}, \end{aligned} \quad (4)$$

where the exponential factor is an approximate fit to the variation of C_{lu} with T_k , valid up to $r \approx 3 \times 10^{16}$ cm. Equations (2) and (4) show that even at $r_{15} = 1$, where $T_k \approx 300$ K, the radiative-to-collisional pumping rate ratio is ~ 2 , and strongly increases with increasing r as a consequence of the diminishing T_k . Figure 4b shows the actual values of Γ_r (dashed line) and Γ_c (solid line) given by the code in model *A*. At $r_{15} = 1$, Γ_r is a factor of ≈ 2 higher than predicted by eq. (2) because dust and gas are mixed and $\langle J \rangle$ is higher than estimated above. The contribution to the excitation of other radiative paths, like $1_{01} \rightarrow \nu_2 2_{12} \rightarrow 2_{21} \rightarrow 1_{10}$ and $2_{12} \rightarrow \nu_2 1_{01} \rightarrow 1_{10}$, accounts for the relatively low o-H₂O abundance required to reproduce the observed 557 GHz flux.

As pointed out in section 2, the inclusion of the $\nu_3 = 1$ state has negligible effect on the line fluxes from the ground vibrational state, which can be shown as follows. The strongest line connecting the 1₀₁ level and the $\nu_3 = 1$ state is the $1_{01} \rightarrow \nu_3 2_{02}$ transition at $\lambda = 2.63 \mu\text{m}$, with a pumping rate per molecule in the 1₀₁ level given by $\Gamma_{r3} \propto \lambda^5 g_{up} A_{ul} F_{2.6 \mu\text{m}}$; here g_{up} is the degeneracy of the upper level of the transition, $A_{ul} \approx 33 \text{ s}^{-1}$ is the Einstein coefficient for spontaneous emission, and $F_{2.6 \mu\text{m}} \approx 0.6 \times 10^{-13} \text{ W cm}^{-2} \mu\text{m}^{-1}$ is the observed 2.6 μm continuum flux. A similar expression applies to the pumping rate in the $1_{01} \rightarrow \nu_2 1_{10}$ transition at 6.2 μm ($A_{ul} \approx 10 \text{ s}^{-1}$), so that the ratio of the pumping rates from the 1₀₁ level into the $\nu_2 1_{10}$ and $\nu_3 2_{02}$ levels is found to be ≈ 55 .

Figure 5 shows the predicted 557 GHz line profiles as observed with HSO (HPBW=41"). Results are given for the telescope pointing toward the source center, and shifted 41" from the source center. In models *A* and *B*, the contribution to the total emission of the outermost regions ($r > 4 \times 10^{16}$ cm, or 16") to the 557 GHz emission is low, and so the line shapes and relative intensity toward the offset position are typical of an optically thick, spatially unresolved line. Model *C* shows, on the contrary, a nearly flat line profile with relatively weak emission toward the source center because the source is partially resolved; in this case the intensity toward the offset position is the strongest of the three models. The predicted line flux and shape within the HSO beam is somewhat dependent on the assumed value of R_{out} , but significant loss of line flux in the wings of the beam is expected in model *C* as long as the source size, $2 \times R_{out}$, is larger than the beam size at 557 GHz, 10^{17} cm (i.e. $R_{out}/R_{int} > 1.25$).

3.2. Predictions for other lines in IRC+10216

The models presented below, showing predictions for H₂O lines other than the 557 GHz one, are the same as those already described in the previous sections, with values for the water vapor abundance such that the o-H₂O 557 GHz line flux observed by SWAS is reproduced for all assumed R_{int} (Fig. 3). Figure 6 shows the energy level diagram of ortho and para-H₂O, and indicates the strongest lines ($\Delta K_{-1} = \pm 1$, $\Delta K_{+1} = \pm 1$) that lie within the HSO-HIFI allowed frequency range. With reference to the energy of the upper level, the lines may be classified into three groups: (i) 8 low-excitation lines, with $E_{up} \lesssim 200$ K; (ii) 3 mid-excitation lines, with $200 \text{ K} < E_{up} \lesssim 300$ K; (iii) 6 high-excitation lines, with $E_{up} > 300$ K ($J_{up} \geq 4$). Figure 7 plots the predicted line fluxes, as observed with the HSO-HIFI beam, versus the inner radius of the H₂O shell, and Fig. 8 shows the expected line profiles for models *A*, *B*, and *C*. Line frequencies and HSO-HIFI beamwidths adopted in these calculations are listed in Table 3.

The overall excitation is, as in the case of the 557 GHz line, dominated by the pumping of the ν_2 state through absorption of 6 μm dust-emitted photons. Nevertheless, absorption of continuum photons in far-infrared pure-rotational transitions also plays an important role in the excitation of some mid- and high-excitation lines. For example, absorption of 45 μm and 58 μm photons in the $\hat{5}23414$ and $\hat{4}22313$ lines, contributes significantly to the excitation of the $\hat{5}23514$ and $\hat{4}22413$ lines, respectively. On the other hand, we find that the effect of collisions is ignorable in all our models. We have run model *A* by quenching off all collisions among rotational levels, and found that the line fluxes vary by less than 4%. Collisional rates much higher than estimated in our extrapolation would be required for collisions to

compete with the radiation field. We conclude that the excitation of H₂O is dominated by the radiation field in all lines and models and our results are dependent on neither the H₂ density nor the T_k profiles, but rely on the adequate simulation of the radiation field generated by dust.

Line fluxes decrease with increasing R_{int} because (i) owing to the decrease of the overall H₂O excitation with increasing distance from the star (Fig. 4a), the emissivity of all lines decreases with increasing R_{int} more steeply than that of the lowest-lying $\hat{1}10101$ transition, and since the SWAS flux of the latter line is kept constant for all R_{int} , all other line fluxes decrease; (ii) for high R_{int} and low-excitation lines, the emission becomes spatially resolved, and hence line flux is lost beyond the wings of the HSO-HIFI beam. The latter effect becomes quite pronounced for high-frequency lines, and explains why the $\hat{2}12101$ line (HPBW=14''5, corresponding to a radius of $\approx 2 \times 10^{16}$ cm) is predicted to be in absorption against the 179.5 μ m continuum emission for $R_{int} \gtrsim 4 \times 10^{16}$ cm (Fig. 8).

Lines belonging to different groups trace different ranges of R_{int} . The low-excitation lines will allow us to check whether H₂O is formed as a result of photodissociation products. If H₂O is formed in the outermost layers of the envelope, with $R_{int} \gtrsim 2 \times 10^{16}$ cm, the 557 GHz line is expected to be the strongest of all lines. Most lines would be undetectable in such a case, given the expected sensitivity of HSO-HIFI (Table 3).

The observation of the high and mid-excitation lines would check whether H₂O is formed in the innermost layers of the envelope. The fluxes predicted for the high-excitation lines decrease by one order of magnitude or more for 4.5×10^{14} cm $\leq R_{int} \leq 2 \times 10^{15}$ cm; however, these high-frequency lines are hardly detectable with the expected sensitivity of HSO-HIFI. Also, the predicted fluxes are somewhat uncertain because they depend on the details of the radiation field in the innermost regions of the envelope, which in turn depend on the distribution and emissivity of dust in these regions. Nevertheless, some mid-excitation lines are still sensitive to low values of R_{int} , as, for example, the $\hat{3}12303$ and $\hat{3}21312$ transitions. These lines, as well as other low-excitation lines, will also probe intermediate values of R_{int} . The fluxes of the $\hat{3}12303$ and $\hat{3}12221$ lines vary by a factor of ≈ 2.5 from $R_{int} = 2 \times 10^{15}$ cm to $R_{int} = 4 \times 10^{15}$ cm, and the flux of the $\hat{3}03212$ line varies by a factor of ≈ 2 in the same R_{int} interval.

The expected line profiles (Fig. 8) display a variety of shapes, from parabolic (optically-thick, spatially-unresolved lines) to triangular (high-excitation lines), double-peaked (spatially-resolved lines), top-hat (optically-thin, spatially-unresolved lines) and P-Cygni (spatially-resolved, ground-state lines) profiles. The greater uncertainty concerns the predicted shapes of the high-excitation lines, as they are formed in the acceleration region.

3.3. HSO observations of C-rich AGB stars other than IRC+10216

In this section we explore the prospects for detecting any of the low-lying ground vibrational state H₂O lines, $\hat{1}10101$ at 557 GHz, $\hat{1}11000$ at 1113 GHz, and $\hat{2}12101$ at 1670 GHz, in C-rich AGB stars other than IRC+10216. Figure 9 shows that, for a source similar to IRC+10216, the line flux ratios depend for high R_{int} on the distance to the source, as a consequence of the spatially extended emission and of the different HSO/HIFI beams available for the three lines (Table 3). For $R_{int} \approx 4 \times 10^{16}$ cm, the 1670 GHz line will only be spatially unresolved if the source is located at more than 2 kpc. We will restrict in the following to models with $R_{int} = 2 \times 10^{15}$ cm, which predict spatially unresolved emission in all lines at essentially any distance. This value of R_{int} corresponds to model *B* in the previous sections, which assumes H₂O to be formed or released at intermediate radii, and whose results for the low-lying lines considered here are also very similar to those obtained for the lowest R_{int} (model *A*, see Table 2).

The role of the mid-IR continuum emission in the excitation of H₂O in IRC+10216 should be also evaluated in other C-rich stars. To this end, we show in Fig. 10a the 6.3 μm mid-IR flux, corrected for the distance, versus the mass loss rate for a sample of C-rich AGB stars. Most \dot{M} and D values have been taken from the compilation of Guandalini et al. (2006). Distance estimates were mostly inferred from HIPPARCOS astrometric measurements by Bergeat, Knapik, & Rutily (2002); the mass loss rates, derived from millimetric molecular observations, were extracted from the literature (e.g., Loup et al. 1993) and subsequently corrected for the updated distances by Bergeat & Chevallerier (2005). Filled symbols in Fig. 10a indicate sources for which the 6.3 μm flux has been directly measured from ISO/SWS spectra (Sloan et al. 2003)¹. The ISO/SWS spectra has also allowed us to determine the 6.3-to-8.8 μm flux density ratio as a function of \dot{M} . This ratio, ranging from 1.25 for the highest \dot{M} to 3.5 for the lowest \dot{M} , has been used to estimate the 6.3 μm fluxes, shown with open symbols, for those sources not observed by ISO/SWS but for which the 8.8 μm flux is available (Guandalini et al. 2006; Monnier et al. 1998; López et al. 1993). The 6.3 μm emission is responsible for the excitation of H₂O through the pumping of the $\nu_2 = 1$ state, and is thus a measure of the impact of the mid-IR emission on the excitation of H₂O. The plot shows that IRC+10216 has a high mid-IR intrinsic luminosity relative to other C-rich stars with similar \dot{M} . In order to simulate the general trend $L_{6.3\mu\text{m}} - \dot{M}$ found for the bulk of sources, we have generated dust models that differ in both \dot{M} and the stellar luminosity (L_*). For the aim of simplicity, only L_* has been varied as a function of \dot{M} , while

¹An Atlas of fully processed ISO/SWS spectra is publicly available at <http://isc.astro.cornell.edu/~sloan/library/swsatlas/atlas.html>

the rest of dust parameters remain equal to those adopted for IRC+10216 (Table 1). The grey line in Fig. 10a shows the fit found with $L_* = 3.5 \times 10^3 L_\odot$ for $\dot{M} = 1.2 \times 10^{-7} M_\odot \text{ yr}^{-1}$, and $L_* = 8 \times 10^3 L_\odot$ for $\dot{M} = 3 \times 10^{-5} M_\odot \text{ yr}^{-1}$.

Figure 10b shows the $6.3 \mu\text{m}$ flux density, corrected for the distance and divided by \dot{M} , as a function of \dot{M} . At any radial position of a given source, the mid-IR radiation density is expected to be proportional to $F_{6.3 \mu\text{m}} D^2$ and the H_2 density proportional to \dot{M} , so that the quantity in the ordinates of Fig. 10b is proportional to the radiative-to-collisional pumping rate ratio. If the kinetic temperature profile is not very different from that adopted for IRC+10216, it is expected that H_2O in those sources with $F_{6.3 \mu\text{m}} D^2 / \dot{M}$ similar to or higher than the value associated with IRC+10216 will be radiatively pumped. Figure 10b shows that radiative pumping is expected to dominate over collisional pumping at least for the bulk of sources with $\dot{M} \lesssim 10^{-5} M_\odot \text{ yr}^{-1}$.

We have used the above dust models to compute the expected H_2O emission as a function of \dot{M} . The key assumption for the H_2O models displayed below is that the H_2O outflow rate (i.e. the total number of H_2O molecules in the envelope) is independent of \dot{M} and equal to the value found in IRC+10216 (which was required to explain the 557 GHz emission). That assumption is appropriate if the origin of the water vapor is the vaporization of icy bodies, because the amount of comets orbiting a star is expected to be independent of \dot{M} , whereas any other formation mechanism involves chemical reactions whose volume rates are proportional to the square of the density. In the cometary hypothesis, the release of H_2O to the outflow is still a function of the stellar luminosity, which is expected to increase with \dot{M} , but also depends on other parameters such as the evolutionary stage of the star after the onset of the TP-AGB phase (Ford & Neufeld 2001), and thus a correlation between the H_2O outflow rate and \dot{M} is uncertain but probably less pronounced than for any other formation mechanism.

Another important model assumption is the parametrization of the photodissociation radius for H_2O molecules, R_{out} , as a function of the mass loss rate. Following Netzer & Knapp (1987), we have assumed that R_{out} scales as $\dot{M}^{0.7}$, but normalized the values of R_{out} in such a way that $R_{out} = 4 \times 10^{17} \text{ cm}$ for $\dot{M} = 3 \times 10^{-5} M_\odot \text{ yr}^{-1}$ (Willacy 2004, AC06). As a result of this different normalization, our values for R_{out} are one order of magnitude larger than the radius of the OH shell calculated by Netzer & Knapp (1987). For high \dot{M} , our resulting values for R_{out} are much larger than the assumed $R_{int} = 2.1 \times 10^{15} \text{ cm}$, and results are not sensitive to the adopted value for R_{out} . However, for $\dot{M} \lesssim 10^{-6} M_\odot \text{ yr}^{-1}$, the finite size for the H_2O shell (e.g. $R_{out}/R_{int} \lesssim 10$) starts to lower the expected line fluxes, in particular that of the 557 GHz line. Since Netzer & Knapp (1987) obtain values for R_{out} that are still much lower than ours, one should consider with caution the H_2O fluxes predicted for $\dot{M} \lesssim 10^{-6}$

$M_{\odot} \text{ yr}^{-1}$. Nevertheless, we note that the photodissociation rate in the unshielded interstellar radiation field ($5.9 \times 10^{-10} \text{ s}^{-1}$) yields, for a 15 km s^{-1} flow, a lengthscale of $\sim 2 \times 10^{15} \text{ cm}$. For $R_{int} = 2 \times 10^{15} \text{ cm}$, this implies a minimum value for R_{out} of $\sim 4 \times 10^{15} \text{ cm}$ for any \dot{M} however small, unless the radiation field is stronger than the average value. For the lowest $\dot{M} = 1.2 \times 10^{-7} M_{\odot} \text{ yr}^{-1}$ considered here, the adopted R_{out} is $8.4 \times 10^{15} \text{ cm}$.

Figure 11 shows the expected fluxes of the three ground-state lines of H_2O as a function of a) \dot{M} , and b) the $6.3 \mu\text{m}$ continuum flux; results are given for a source at $D = 0.5 \text{ kpc}$. We find that the excitation is dominated by absorption of mid-IR photons; only for the highest \dot{M} does collisional excitation account for at most 20% of the predicted flux in the ground-state lines. Therefore, a tight correlation between line fluxes and the $6.3 \mu\text{m}$ continuum flux density is found in Fig. 11b, where fits of the form $F \propto F_{6.3\mu\text{m}}^b$ are displayed. The slope b is ≈ 1 for the 1670 GHz line, but somewhat lower for the 557 and 1113 GHz lines (0.87 and 0.94, respectively) due to slight opacity effects in the vibrational lines responsible for the radiative pumping. The slopes would approach to unity for a microturbulent velocity higher than the assumed value of 0.65 km s^{-1} . For low \dot{M} , the data points are slightly below the fitted lines as a result of the H_2O photodissociation effects mentioned above; stronger departures from the fitted lines are expected for lower values of R_{out} .

According to the current estimates of the HSO-HIFI sensitivities (Table 3), the 557 GHz line will be detected in 1.5 hours at more than 5σ level if the line flux is higher than $1.3 \times 10^{-22} \text{ W cm}^{-2}$ (after coadding the two polarization modes). From Fig. 11b, this sensitivity limit translates into a $6.3 \mu\text{m}$ flux density of $1.7 \times 10^{-15} \text{ W cm}^{-2} \mu\text{m}^{-1}$ at $D = 0.5 \text{ kpc}$, which can be in turn adapted to any other distance provided that both the line and continuum fluxes vary as D^{-2} . Figure 11c shows the $6.3 \mu\text{m}$ fluxes for the sample of C-rich AGB stars, with the solid line indicating the $6.3 \mu\text{m}$ flux density required to detect the 557 GHz line according to the quoted sensitivity limit. *All sources above the solid line would be detected with 1.5 hours of observing time in the 557 GHz line if the H_2O outflow rate were equal or higher than the value found in IRC+10216, and if the photodissociation radius of the H_2O molecules remains sufficiently large relative to R_{int} .* The sensitivity limits for the 1113 and 1670 GHz lines are also displayed, and show that the detection of these lines require significantly higher $6.3 \mu\text{m}$ continuum fluxes. We conclude that the 557 GHz line provides the most sensitive means of searching for H_2O in C-rich AGB stars other than IRC+10216 with HSO.

4. Discussion

4.1. Model uncertainties

Our models for IRC+10216 predict that, whatever the region where H₂O is formed or released to the outflow, H₂O is radiatively excited, which implies that model results are independent of the gas temperature and density profiles. This result relies on the extrapolation to higher T_k of the collisional rates given by Phillips et al. (1996), which will require further confirmation from new estimates of H₂O-H₂ collisional rates at higher temperatures. Nevertheless, we find that collisional rates would have to be about one order of magnitude higher than estimated to compete efficiently with the radiative rates in the innermost regions of the envelope, which seems somewhat implausible.

A relatively uncertain parameter in our models is the assumed distance to IRC+10216, $D = 170$ pc. It has been proposed that the distance may be substantially smaller, $D = 100 - 150$ pc (Zuckerman, Dyck, & Claussen 1986; Groenewegen et al. 1992). At 170 pc, the inferred stellar luminosity is $L_* \approx 2 \times 10^4 L_\odot$, which results in $L_* \approx 10^4 L_\odot$ at $D = 120$ pc, a value more similar to the inferred luminosities of other C-rich AGB stars with similar \dot{M} (Schöier, Olofsson, & Lundgren 2006). If $D = 120$ pc, both \dot{M} and the radiation density at $6 \mu\text{m}$ are a factor of 2 lower than assumed, so that the radiative-to-collisional pumping rate ratio still remains unchanged. Since the closer proximity and weaker $6 \mu\text{m}$ radiation density have opposite effects on the H₂O outflow rate required to match the SWAS 557 GHz flux, the latter will decrease by less than a factor 2, and thus the expected H₂O abundance will be a factor of < 2 higher than in Table 2. Therefore, we conservatively estimate an o-H₂O abundance in the range $(0.5 - 1) \times 10^{-7}$ for $R_{int} = 2 \times 10^{15}$ cm. Concerning the line ratios to be observed by HSO, we expect values similar to those obtained at $D = 170$ pc if the line emission remains unresolved, i.e. for low values of R_{int} . For high values of R_{int} , beam effects will be more important at $D = 120$ pc, diminishing the low-excitation line fluxes relative to the 557 GHz line.

A potentially more important source of uncertainty is the assumption of spherical symmetry in our models. Both the molecular and dust emission from IRC+10216 show evidence for departures from a smooth distribution in a spherically symmetric outflow; incomplete, discrete shells or arcs and clumpy structures are instead observed on a wide range of distances to the star (e.g. Lucas & Guélin 1999; Mauron & Huggins 1999; Fong, Meixner, & Shah 2003; Leão et al. 2006). Even more important, the OH line shapes observed in IRC+10216 strongly suggest an asymmetric distribution of OH in the outer regions of the envelope (Ford et al. 2003), thus also suggesting an asymmetric distribution of the parent H₂O molecule. These asymmetries may alter to some extent the H₂O line flux ratios calculated with the use of

our spherically symmetric approach. While in spherical symmetry the emission from any line is isotropic, in filamentary structures or slabs of velocity-coherent gas the optically thick lines radiate preferentially in the direction perpendicular to the two faces of the sheet (Elitzur, Hollenbach, & McKee 1989), whereas the emission from thinner lines will approach a more isotropic behavior. Future HSO observations will show the importance of the observed morphological complexity on the line fluxes by showing whether the different H₂O line flux ratios are consistent with a single value of R_{int} , or indicate a range of values.

Finally, the models assume a water shell with uniform H₂O abundance and sharp inner and outer radii; however, a finite abundance gradient obviously takes place at both the H₂O formation and dissociation regions, and variations of the H₂O abundance across the shell are also possible. These effects may also alter to some extent the expected line flux ratios. Uncertainties in the outer radius of the H₂O shell may also affect the expected fluxes from stars with low mass loss rates.

4.2. Water formation at inner or intermediate radii

Both the cometary and Fischer-Tropsch catalysis hypothesis predict H₂O to be released or formed at intermediate radii of *a few* $\times 10^{15}$ cm, and although no specific mechanism has been proposed for H₂O formation at the innermost regions ($R_{int} < 10^{15}$ cm), this possibility cannot be rejected. The models shown in section 3.2 will permit us to discriminate, from HSO observations of IRC+10216, if there are significant amounts of H₂O in the innermost regions through the observation of mid-excitation H₂O transitions. More difficult will be a priori to discriminate between the cometary and Fischer-Tropsch catalysis propositions. Both predict similar values for R_{int} ; nevertheless, if R_{int} were found to be significantly higher than 2×10^{15} cm, the release of H₂O from comets could be favoured, unless some additional mechanism were found to shift R_{int} , within the Fischer-Tropsch catalysis framework (Willacy 2004), outwards in the envelope. The search for water emission at 557 GHz in C-rich AGB stars other than IRC+10216 will also favour one of the two hypotheses: since IRC+10216 is at the high end of mass loss rates from C-rich stars, and the efficiency of Fischer-Tropsch catalysis to form H₂O molecules is expected to decrease with diminishing \dot{M} , one would expect in such a case a rate of detection significantly lower than that quantified in section 3.3 for the cometary hypothesis, and one would expect a pronounced decline of the H₂O abundance with diminishing \dot{M} .

The ISO/LWS spectrum of IRC+10216 (Cernicharo et al. 1996) shows an emission feature at 179.5 μm , coincident with the wavelength of the $\hat{2}12101$ o-H₂O transition, with a flux of $\approx 8 \times 10^{-20}$ W cm⁻². This flux is very similar to that computed for the quoted line

in model *B* ($R_{int} = 2.1 \times 10^{15}$ cm). However, the far-infrared spectrum of IRC+10216 shows vibrationally excited rotational emission of HCN, and the combined emission of the $\nu_1 = 1$ $J = 19 \rightarrow 18$ and $\nu_3 = 1$ $J = 19 \rightarrow 18$ HCN lines, both emitting at $179.5 \mu\text{m}$, is expected to be also comparable to the measured line flux at $179.5 \mu\text{m}$ (Cernicharo et al. 1996). Given the uncertainties inherent to the HCN model in Cernicharo et al. (1996), where the excited vibrational states are assumed to be thermalized, and given the high density of spectral lines in the IRC+10216 far-infrared spectrum, which makes it difficult to establish the contribution from the $\nu_1 = 1$ and $\nu_3 = 1$ rotational lines to the spectrum, the relative contribution from HCN and H_2O to the observed spectral feature is quite uncertain. On the other hand, the expected flux of the $\bar{3}03212$ line at $174.6 \mu\text{m}$ in model *B* is $\approx 4 \times 10^{-20} \text{ W cm}^{-2}$, below the $3\text{-}\sigma$ upper limit derived for that line from the ISO/LWS spectrum. These considerations suggest weakly that H_2O in IRC+10216 is formed or released at radial distances $R_{int} \gtrsim 2 \times 10^{15}$ cm.

Our models show that the required H_2O abundance for R_{int} in the range $(2 - 5) \times 10^{15}$ cm is $(0.5 - 1) \times 10^{-7}$ relative to H_2 , which makes the requirements previously demanded for the cometary and Fischer-Tropsch catalysis hypothesis to work in IRC+10216 less restrictive (Ford & Neufeld 2001; Willacy 2004). The water outflow rate is $(0.5 - 1) \times 10^{-5} M_{\oplus} \text{ yr}^{-1}$, which yields, within the framework of vaporization of icy bodies, a required total initial ice mass of $(0.5 - 10) M_{\oplus}$ for $\dot{M}(\text{H}_2\text{O})/M_0(\text{ice})$ in the range $10^{-5} - 10^{-6} \text{ yr}^{-1}$ (Ford & Neufeld 2001). On the other hand, the Fischer-Tropsch catalysis on metallic grains will require a density of iron grains relative to total H nuclei of $n_g(\text{Fe})/n_{\text{H}} = (0.5 - 1) \times 10^{-13}$ to explain the observed H_2O 557 GHz emission (Willacy 2004).

4.3. Water formation in the outermost layers

Multitransition HSO observations of H_2O in IRC+10216 will easily establish whether or not water is formed in the external layers of the envelope; the predicted fluxes in Fig. 7 and the HSO-HIFI sensitivities in Table 3 indicate that only the $\hat{1}10101$ o- H_2O line, and possibly the $\hat{1}11000$ and $\hat{2}02111$ p- H_2O lines, are detectable in one hour of observing time for $R_{int} \gtrsim 4 \times 10^{16}$ cm.

For high R_{int} , the expected flux in the 557 GHz line can be obtained analytically. Since essentially all o- H_2O molecules are in the ground 1_{01} level (Fig. 4a), the o- H_2O $\hat{1}10101$ line flux is derived from the radiative pumping rate given in eq. (2) after multiplying Γ_r by 1.35 to account for the two radiative pumping routes that are relevant at high distances from the star (Fig. 4b):

$$F(1_{10} \rightarrow 1_{01}) = 1.4 \times 10^{-21} \times \left(\frac{4 \times 10^{17} \text{ cm}}{R_{out}} \right)$$

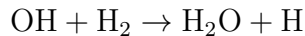
$$\times \left(\frac{R_{out}}{R_{int}} - 1 \right) \times \left(\frac{X(o - H_2O)}{5 \times 10^{-7}} \right) \frac{W}{\text{cm}^2}, \quad (5)$$

where X is the abundance relative to H_2 . Equation (5) is independent of the assumed distance D to the star because, in order to match the observed mid-IR continuum, $\Gamma_r \propto D^2$ (eq. 1); it assumes a water shell with sharp edges at R_{int} and R_{out} and constant H_2O abundance; it ignores slight opacity effects in the ro-vibrational lines (section 3.1) as well as beam effects (both slightly raise the required abundance), and overestimates by less than 20% the 557 GHz line flux obtained in model C . In the limit $R_{out} \rightarrow \infty$, and using $F(1_{10} \rightarrow 1_{01}) = 10^{-20}$ $W \text{ cm}^{-2}$ (Melnick et al. 2001), eq. (5) gives

$$\chi(H_2O) \gtrsim 2.4 \times 10^{-7} \times \left(\frac{R_{int}}{4 \times 10^{16} \text{ cm}} \right), \quad (6)$$

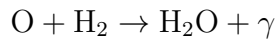
where $\chi(H_2O)$ is here the H_2O (ortho+para) abundance relative to H nuclei. Equation 6 gives the sharp-inner edge, lower limit for the H_2O abundance required to account for the observed 557 GHz line flux, as a function of R_{int} . AC06 have reported an abundance of $\chi(H_2O) \sim 10^{-7}$ to account for the observed 557 GHz line flux in IRC+10216. However, the quoted abundance would imply an inner radius of $R_{int} \lesssim 2 \times 10^{16}$ cm, but the H_2O abundance shown by AC06 (their Fig. 7) decreases sharply at $r < 4 \times 10^{16}$ cm. Based on detailed modelling, we indicate that the $\chi(H_2O)$ profile given by AC06 has to be shifted up by a factor of ≈ 2.5 to account more accurately for the 557 GHz line flux measured by SWAS.

In the model proposed by AC06, atomic oxygen is produced in a shell by the photodissociation of CO (and particularly the ^{13}CO isotopologue, which shields itself far less effectively than ^{12}CO .) Since the temperature is low (~ 10 K) within the shell where the atomic oxygen abundance is significant, the neutral-neutral reaction sequence



is very slow –and therefore is negligible as a source of H_2O – the first reaction being endothermic and the second –although exothermic– possessing a substantial activation energy barrier.

AC06 therefore proposed the radiative association reaction



as an alternative source of H_2O . To match the SWAS- and ODIN-observed water line fluxes, AC06 had to posit that this reaction is relatively rapid at low temperature, with a rate

coefficient $k_{ra} \sim 10^{-15} \text{ cm}^3 \text{ s}^{-1}$. According to our estimation above, k_{ra} has to be a factor ≈ 2.5 higher than this value to account for the measured $\hat{1}10101$ H_2O flux. Nevertheless, and even with the use of the k_{ra} estimation given by AC06, we find that this large reaction rate coefficient for the radiative association of O and H_2 is inconsistent with observations of H_2O and OH in at least one translucent molecular cloud, for which sufficient data exist to disipate any significant ambiguity: observations of the cloud along the sight-line to HD 154368 –carried out by Spaans et al. (1998) with the use of the Goddard High Resolution Spectrograph (GHRS) on the *Hubble Space Telescope* (HST) – yield a 3σ upper limit on the water abundance that lies almost two orders of magnitude below the value that would obtain were k_{ra} as large as $10^{-15} \text{ cm}^3 \text{ s}^{-1}$. The factor of discrepancy would rise above 150 for $k_{ra} \approx 2.5 \times 10^{-15} \text{ cm}^3 \text{ s}^{-1}$.

The best-fit model for the HD 154368 cloud obtained by Spaans et al. (1998) posits a plane parallel cloud of total visual extinction $A_V = 2.65$ mag in which the density of H nuclei is $n_{\text{H}} = 325 \text{ cm}^{-3}$ (this is probably a lower limit at the cloud center, as the density inferred from the CO $J = 1 \rightarrow 0/3 \rightarrow 2$ ratio is $\sim 10^3 \text{ cm}^{-3}$; see van Dishoeck et al. 1991) and the external ultraviolet radiation field is 3 times mean interstellar value given by Draine (1978): $I_{UV} = 3$. Under these conditions, the destruction of H_2O is dominated by photodissociation at a rate $\zeta = 5.9 \times 10^{-10} \text{ s}^{-1} \times I_{UV} \times (\exp\{-1.7A_{V1}\} + \exp\{-1.7A_{V2}\})/2$ (Le Teuff, Millar, & Markwick 2000)², where A_{V1} is the visual extinction to one cloud surface and $A_{V2} = 2.65 - A_{V1}$ is the extinction to the other. At the cloud center, the water photodissociation rate is $1.9 \times 10^{-10} \text{ s}^{-1}$.

For a radiative association rate of k_{ra} , the ratio of water vapor to atomic oxygen is therefore given by the expression

$$n(\text{H}_2\text{O})/n(\text{O}) = k_{ra}n_{\text{H}}f_{\text{H}_2}/\zeta,$$

where $f_{\text{H}_2} \equiv n(\text{H}_2)/n_{\text{H}}$. At the cloud center, the cloud is almost fully molecular, with $f_{\text{H}_2} \sim 0.5$, and the above equation yields $n(\text{H}_2\text{O})/n(\text{O}) = 8.7 \times 10^{-4} (k_{ra}/10^{-15} \text{ cm}^3 \text{ s}^{-1})$. In Fig. 12, we show the predicted $n(\text{H}_2)/n_{\text{H}}$ ratio for the best-fit Spaans et al. (1998) model, together with the $n(\text{H}_2\text{O})/n(\text{O})$ ratio that would result if k_{ra} were $10^{-15} \text{ cm}^3 \text{ s}^{-1}$. The model predicts hydrogen to be predominantly in molecular form, in agreement with results by Snow et al. (1996). Averaging the $n(\text{H}_2\text{O})/n(\text{O})$ ratio over the entire sight-line, we obtain a column density ratio $N(\text{H}_2\text{O})/N(\text{O}) = 5.3 \times 10^{-4} (k_{ra}/10^{-15} \text{ cm}^3 \text{ s}^{-1})$.

²We note that the factor of 1.7 in the exponential, widely used in the literature, yields H_2O photodissociation rates at the midplane of the plane-parallel cloud that are higher than the values reported by Roberge et al. (1991) by factors of 2.2 and 10 for $A_V^{tot} = 1$ mag and $A_V^{tot} = 10$ mag, respectively; therefore, our estimation for the $N(\text{H}_2\text{O})/N(\text{O})$ ratio predicted by the radiative association of O and H_2 is probably a conservative lower limit.

The atomic oxygen column density along the HD 154368 sight-line is $N(\text{O}) = 1.2 \times 10^{18} \text{ cm}^{-2}$ (Snow et al. 1996, from absorption line observations of the 1355 \AA OI] line). Based on a search for the $C^1B_1 - X^1A_1$ band of water vapor near 1240 \AA , Spaans et al. (1998) obtained 3σ upper limit on the water column density of $9 \times 10^{12} \text{ cm}^{-2}$, corresponding to $N(\text{H}_2\text{O})/N(\text{O}) = 7.5 \times 10^{-6}$. This 3σ upper limit lies a factor 70 below the value that we would obtain were k_{ra} equal to $10^{-15} \text{ cm}^3 \text{ s}^{-1}$ as AC06 suggested, and places a 3σ upper limit of $1.4 \times 10^{-17} \text{ cm}^3 \text{ s}^{-1}$ on k_{ra} .

AC06 suggested that the freeze out of oxygen onto grain mantles could diminish the water vapor abundance in molecular clouds, as proposed by Bergin et al. (2000) to explain the low H_2O abundances measured by SWAS in dense clouds. Ice absorption line observations of diffuse/translucent sight-lines, however, indicate that water ice is generally present only in clouds of $A_V \geq 3$ (Whittet et al. 2001). Furthermore, in the specific case of HD 154368 under present consideration, the atomic oxygen is known from direct measurement to be $1.2 \times 10^{18} \text{ cm}^{-2}$. The column density of H nuclei along this sight-line, $N_{\text{H}} = N(\text{H}) + 2N(\text{H}_2)$, has been measured to be $4.2 \times 10^{21} \text{ cm}^{-2}$ (Snow et al. 1996), so the mean line-of-sight oxygen abundance is $n(\text{O})/n_{\text{H}} \sim 3 \times 10^{-4}$, a value that is entirely consistent with the abundances measured along diffuse sight-lines (Meyer et al. 1998) and inconsistent with a significant depletion of oxygen onto ice mantles.

In summary, the upper limit on the water vapor abundance observed towards HD 154368 definitively rules out a rate coefficient for the radiative association reaction $\text{O} + \text{H}_2 \rightarrow \text{H}_2\text{O} + \gamma$ that is large enough to explain –in the context of the AC06 model– the $\text{H}_2\text{O} \hat{1}10101$ line strength measured by SWAS toward IRC+10216. If HSO observations would indicate that H_2O is formed in the external layers of IRC+10216, an explanation other than the radiative association proposed by AC06 would be required to avoid incompatibilities with observations toward HD 154368.

5. Summary

Our radiative transfer models for H_2O in IRC+10216 and other C-rich AGB stars reveal:

- 1) H_2O in the envelope of IRC+10216 is primarily excited through absorption of photons in the ν_2 band at $6 \mu\text{m}$ and subsequent decay to the ground vibrational state.
- 2) The o- H_2O abundance relative to H_2 required to account for the $557 \text{ GHz} \hat{1}10101$ o- H_2O line observed in IRC+10216 is in the range $(0.5 - 5) \times 10^{-7}$, depending on the inner radius of the H_2O shell.
- 3) Multitransition H_2O observations with the Herschel Space Observatory will allow us to establish the spatial distribution of H_2O molecules in IRC+10216, in particular the inner

radius of the H₂O shell, thus discriminating among the different hypothesis proposed for the origin (formation or release) of H₂O.

4) A number of other C-rich AGB stars with relatively strong 6 μ m continuum flux are expected to be detectable in the $\hat{1}10101$ o-H₂O line with HSO, if the H₂O outflow rate in those sources is similar to that found in IRC+10216.

5) The relatively low H₂O abundance required to explain the $\hat{1}10101$ o-H₂O emission in IRC+10216 makes less restrictive the requirements previously reported for the vaporization of icy bodies or Fischer-Tropsch catalysis on the surfaces of metallic grains to work. If H₂O were formed in the external layers of IRC+10216, we find that an explanation for the H₂O formation other than the previously reported radiative association $O + H_2 \rightarrow H_2O + \gamma$ is required to avoid conflict with observations of the translucent cloud towards HD 154368.

D.A.N. gratefully acknowledges the support of grant NAG 5 - 13114 from NASA's Long Term Space Astrophysics research program. This research has made use of NASA's Astrophysics Data System.

REFERENCES

- Agúndez, M., & Cernicharo, J. 2006, ApJ, 650, 374 (AC06)
- Bagnulo, S., Doyle, J.G., & Griffin, L.P. 1995, A&A, 301, 501
- Bergeat, J., Knapik, A., & Rutily B. 2002, A&A, 390, 967
- Bergeat, J., & Chevallier, L. 2005, A&A, 429, 235
- Bergin, E.A., Melnick, G.J., Stauffer, J.R., et al. 2000, ApJ, 539, L129
- Cernicharo, J., Barlow, M.J., González-Alfonso, E., et al. 1996, A&A, 315, L201
- Dinh-V-Trung, & Nguyen-Q-Rieu 2000, A&A, 361, 601
- Draine, B.T. 1978, ApJS, 36, 595
- Elitzur, M., Hollenbach, D.J., McKee, C.F. 1989, ApJ, 346, 983
- Fong, D., Meixner, M., & Shah, R.Y. 2003, ApJ, 582, L39
- Ford, K.E.S., Neufeld, D.A. 2001, ApJ, 557, L113
- Ford, K.E.S., Neufeld, D.A., Goldsmith, P.F., & Melnick, G.J. 2003, ApJ, 589, 430

- Ford, K.E.S., Neufeld, D.A., Schilke, P., & Melnick, G.J. 2004, *ApJ*, 614, 990
- Glassgold, A.E. 1996, *ARAA*, 34, 241
- González-Alfonso, E., & Cernicharo, J. 1997, *A&A*, 322, 938
- González-Alfonso, E., & Cernicharo, J. 1999, *ESA SP-427*, “The Universe as seen by ISO”, 325
- González-Alfonso, E., & Cernicharo, J. 1999, *ApJ*, 525, 845
- Green, S., Maluendes, S., & McLean, A.D. 1993, *ApJS*, 85, 181
- Groenewegen, M.A.T., de Jong, T., van der Blik, N.S., Slijkhuis, & S., Willems, F.J. 1992, *A&A*, 253, 150
- Guandalini, R., Busso, M., Ciprini, S., Silvestro, G., & Persi, P. 2006, *A&A*, 445, 1069
- Hasegawa, T.I., Kwok, S., Koning, N., et al. 2006, *ApJ*, 637, 791
- Kwan, J., & Linke, R.A. 1982, *ApJ*, 254, 587
- Leão, I.C., de Laverny, P., Mékarnia, D., de Medeiros, J.R., & Vandame, B. 2006, *A&A*, 455, 187
- Le Teuff, Y.H., Millar, T.J., & Markwick, A.J. 2000, *A&AS*, 146, 157
- López, B., Perrier, C., Mekarnia, D., Lefevre, J., & Gay, J. 1993, *A&A*, 270, 462
- Loup, C., Forveille, T., Omont, A., & Paul, J.F. 1993, *A&AS*, 99, 291
- Lucas, R., Guélin, M. 1999, in *IAU Symposium 191*, Ed. by Le Bertre, T., Lebre, A., & Waelkens, C. IAU & Astr. Soc. of the Pacific, p. 305
- Mauron, N., & Huggins, P.J. 1999, *A&A*, 349, 203
- Melnick, G.J., Neufeld, D.A., Ford, K.E.S., Hollenbach, D.J., Ashby, M.L.N. 2001, *Nature*, 412, 160
- Meyer, D.M., Jura, M., & Cardelli, J.A. 1998, *ApJ*, 493, 222
- Monnier, J.D., Geballe, T.R., & Danchi, W.C. 1998, *ApJ*, 502, 833
- Netzer, N., & Knapp, G.R. 1987, *ApJ*, 323, 734
- Phillips, T.R., Maluendes, S., & Green, S. 1996, *ApJS*, 107, 467

- Roberge, W.G., Jones, D., Lepp, S., & Dalgarno, A. 1991, *ApJS*, 77, 287
- Rothman, L.S., et al. 2005, *Journal of Quantitative Spectroscopy & Radiative Transfer*, 96, 139
- Schöier, F.L., Olofsson, H., & Lundgren, A.A. 2006, *A&A*, 454, 247
- Schönberg, K., & Kempe, K. 1986, *A&A*, 163, 151
- Sloan, G.C., Kraemer, K.E., Price, S.D., & Shipman, R.F. 2003, *ApJS*, 147, 379
- Snow, T.P., Black, J.H., van Dishoeck, E.F., Burks, G., Crutcher, R.M., Lutz, B.L., Hanson, M.M., & Shuping, R.Y. 1996, *ApJ*, 465, 245
- Spaans, M., Neufeld, D., Lepp, S., Melnick, G.J., & Stauffer, J. 1998, *ApJ*, 503, 780
- Tenenbaum, E.D., Apponi, A.J., Ziurys, L.M., Agúndez, M., Cernicharo, J., Pardo, J.R., & Guélin, M. 2006, *ApJ*, 649, L17
- van Dishoeck, E.F., Phillips, T.G., Black, J.H., & Gredel, R. 1991, *ApJ*, 366, 141
- Whittet, D.C.B., Gerakines, P.A., Hough, J.H., & Shenoy, S.S. 2001, *ApJ*, 547, 872
- Willacy, K. 2004, *ApJ*, 600, L87
- Zuckerman, B., Dyck, H.M., & Claussen, M.J. 1986, *ApJ*, 304, 401

Table 1. Model parameters for IRC+10216 ^a

Parameter	Value
Gas velocity field	$v(r) = 14.5\sqrt{1 - 0.95\frac{R_i}{r}}$ km s ⁻¹
Turbulent velocity	$v_t = 0.65$ km s ⁻¹
H ₂ density	$n(\text{H}_2) = \frac{3.11 \times 10^7}{r_{15}^2} \frac{14.5 \text{ kms}^{-1}}{v(r)}$ cm ⁻³
Gas temperature	$T_k(r) = 12 \left(\frac{90}{r_{15}}\right)^{0.72}$ K if $r_{15} < 110$ $T_k(r) = 10$ K if $r_{15} > 110$
Dust inner radius	$R_i = 4.5 \times 10^{14}$ cm
Dust outer radius	$R_o = 4.0 \times 10^{17}$ cm
Stellar radius	$R_* = 8.0 \times 10^{13}$ cm
Stellar temperature	$T_* = 2050$ K
Spectral index	$\beta = 1.3$ if $\lambda > 20 \mu\text{m}$ $\beta = 1$ if $\lambda < 20 \mu\text{m}$

^a r is the distance to the star in cm, and $r_{15} = \frac{r}{10^{15}\text{cm}}$.

Table 2. Inner and outer radii for the H₂O shell in different models, and derived o-H₂O abundances

Model	R_{int} (cm)	R_{out} (cm)	$X(\text{o-H}_2\text{O})^a$
<i>A</i>	4.5×10^{14}	4.0×10^{17}	4.1×10^{-8}
<i>B</i>	2.1×10^{15}	4.0×10^{17}	5.4×10^{-8}
<i>C</i>	4.3×10^{16}	4.0×10^{17}	5.1×10^{-7}

^ao-H₂O abundances are given relative to H₂, and an ortho-to-para H₂O abundance ratio of 3:1 is assumed in all models.

Table 3. H₂O transitions, frequencies, and adopted HSO-HIFI half-power beamwidths and sensitivities

Transition	Frequency (GHz)	HSO-HIFI beam ^a ($''$)	Sensitivity ^b (10^{-22} W cm ⁻²)
$\hat{1}10101$	556.9	41.0	2.2
$\hat{3}12303$	1097.4	21.0	12
$\hat{3}12221$	1153.1	18.5	29
$\hat{3}21312$	1162.9	18.5	30
$\hat{5}23514$	1410.6	14.5	45
$\hat{2}21212$	1661.0	14.5	61
$\hat{2}12101$	1669.9	14.5	62
$\hat{3}03212$	1716.8	12.5	56
$\hat{5}32523$	1867.7	12.5	65
$\hat{2}11202$	752.0	29.0	4.1
$\hat{2}02111$	987.9	21.0	9.2
$\hat{1}11000$	1113.3	21.0	12
$\hat{4}22413$	1207.6	18.5	32
$\hat{2}20211$	1228.8	18.5	35
$\hat{4}13404$	1602.2	14.5	55
$\hat{6}33624$	1762.0	12.5	60
$\hat{6}24615$	1794.8	12.5	64

^aAdopted from <http://www.ipac.caltech.edu/Herschel/hifi/hifi.shtml>

^bCalculated using HSPOT version 1.9.1; sensitivities correspond to 5σ in 1 hr with a spectral resolving power of $R = 10^4$

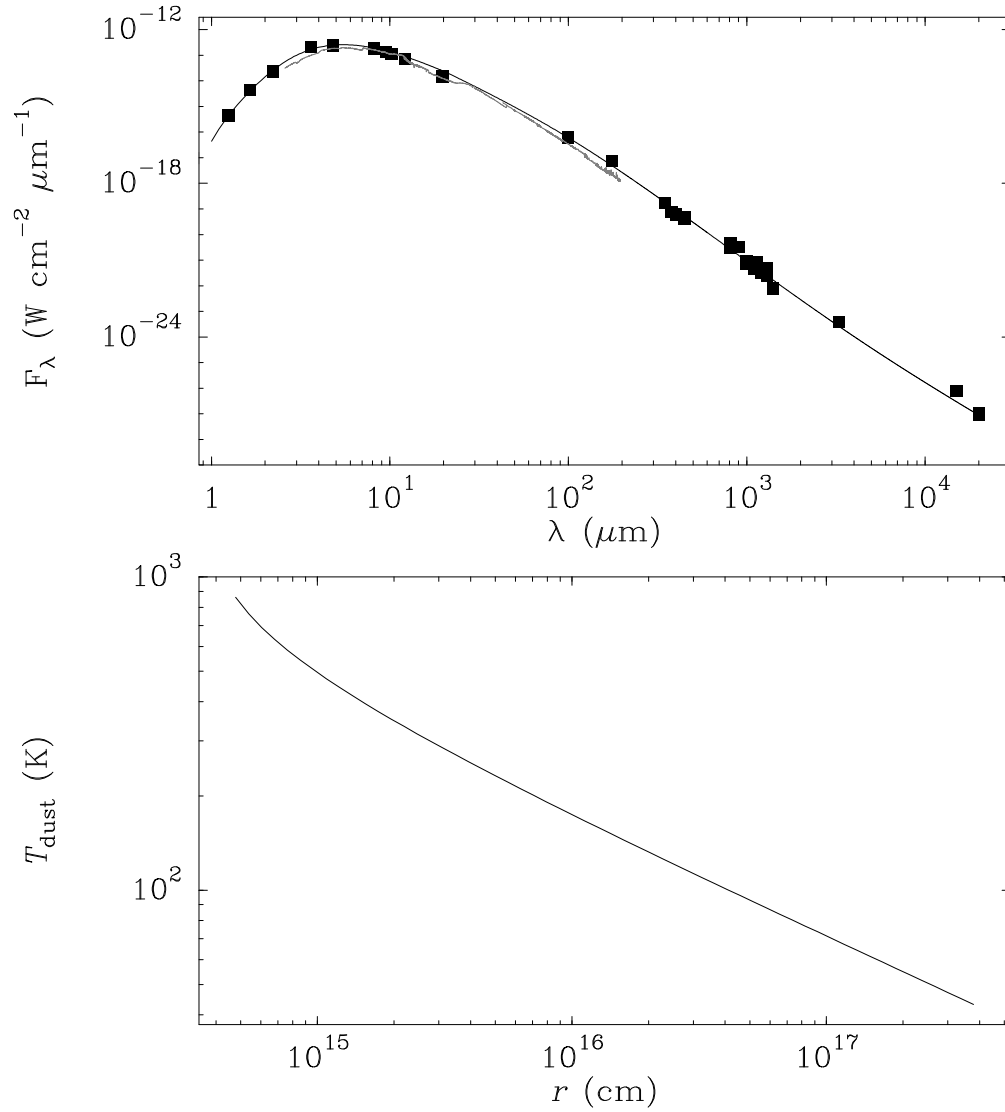


Fig. 1.— *Top*: Fit to the continuum emission from IRC+10216. Data points are taken from Bagnulo et al. (1995), and the grey line shows the ISO data. *Bottom*: Dust temperature profile.

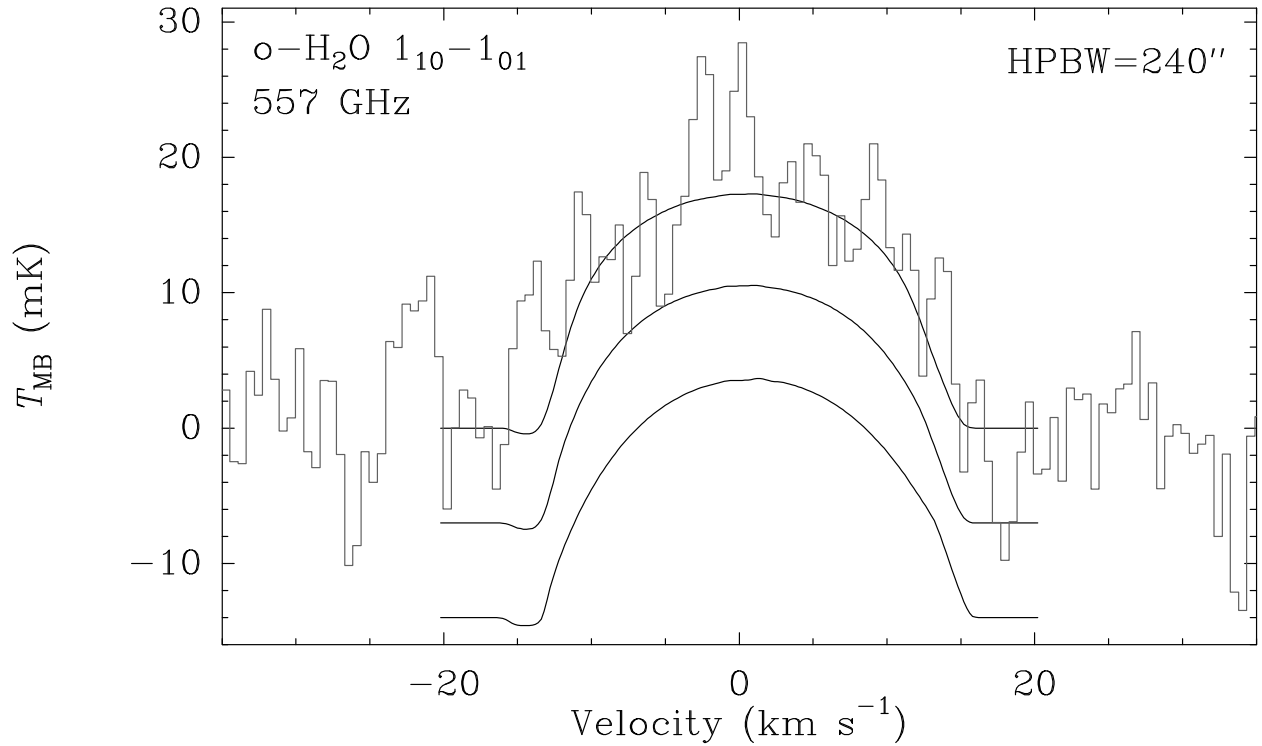


Fig. 2.— Comparison between the SWAS $\hat{1}10101$ o-H₂O spectrum (from Melnick et al. 2001) and the line profile obtained for models *A* (upper), *B* (middle), and *C* (lower), with the SWAS beamsize. The spectra of models *B* and *C* have been shifted vertically for clarity. The required abundances of o-H₂O are given in Table 2.

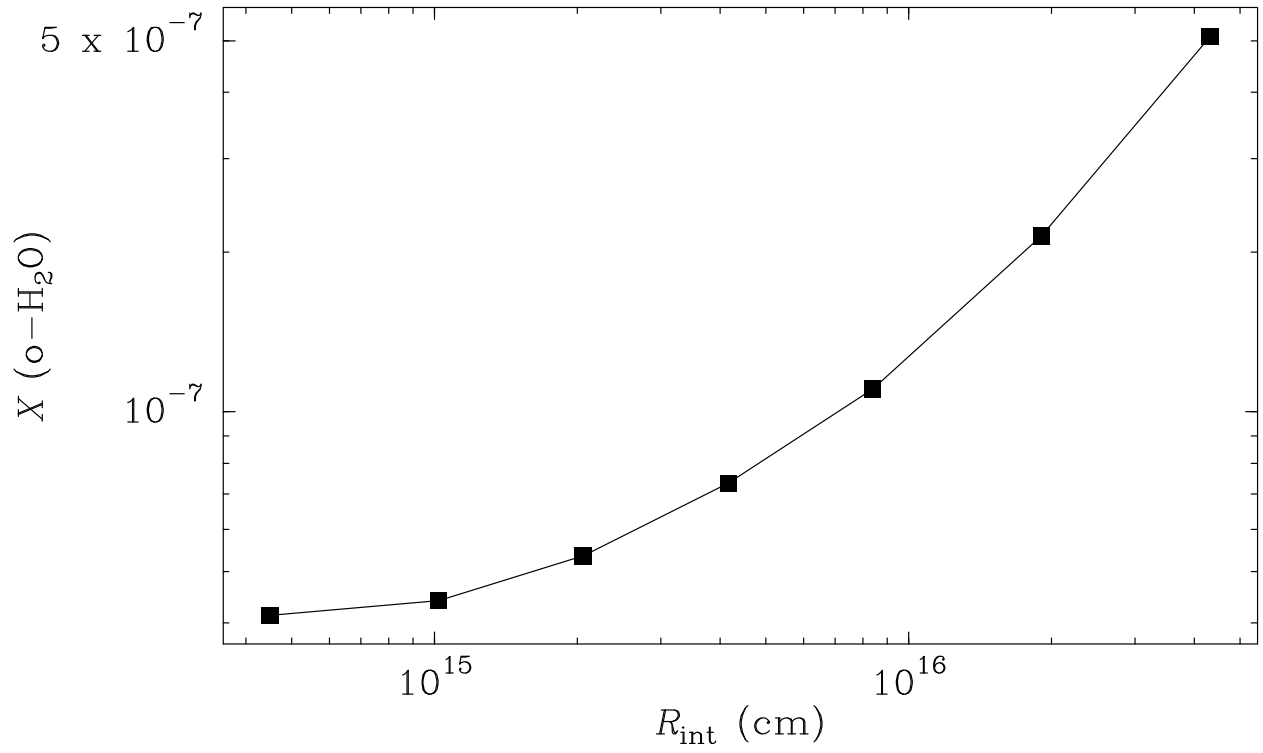


Fig. 3.— Ortho-H₂O abundance, relative to H₂, required to account for the observed 557 GHz H₂O emission in IRC+10216, as a function of the assumed inner radius of the H₂O shell.

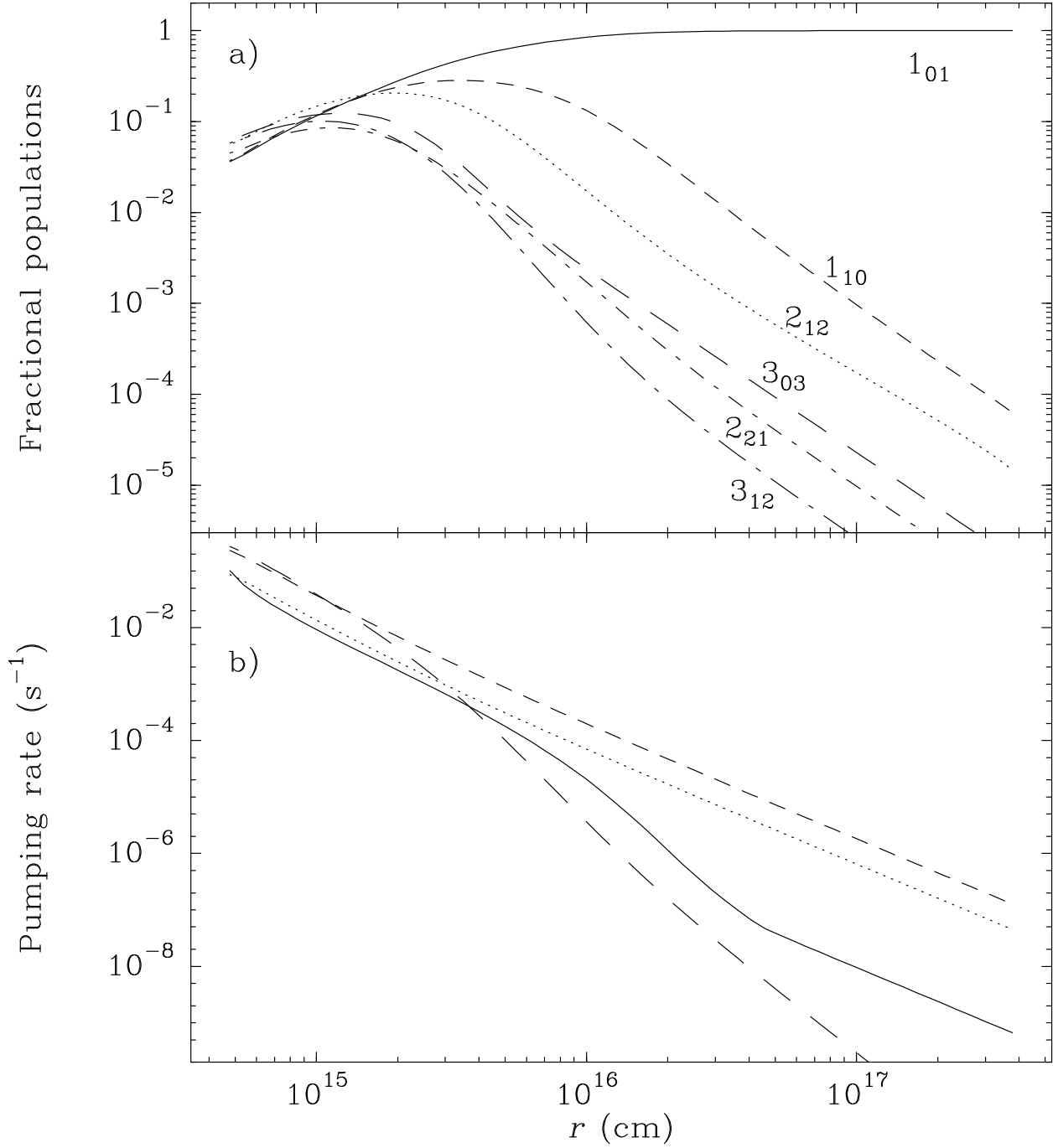


Fig. 4.— a) Fractional populations of the 6 lowest energy levels of ortho-H₂O in model A; b) collisional and radiative pumping rates, per molecule in the 1_{01} level, for the 1_{10} level in model A. Solid line: collisional pumping, which is computed from the $1_{01} \rightarrow 1_{10}$ collisional rate; dashed line: radiative rate through the path $1_{01} \rightarrow \nu_2 1_{10} \rightarrow 2_{21} \rightarrow 1_{10}$; dotted line: radiative rate through the path $1_{01} \rightarrow \nu_2 2_{12} \rightarrow 2_{21} \rightarrow 1_{10}$; long-dashed line: radiative rate through the path $2_{12} \rightarrow \nu_2 1_{01} \rightarrow 1_{10}$.

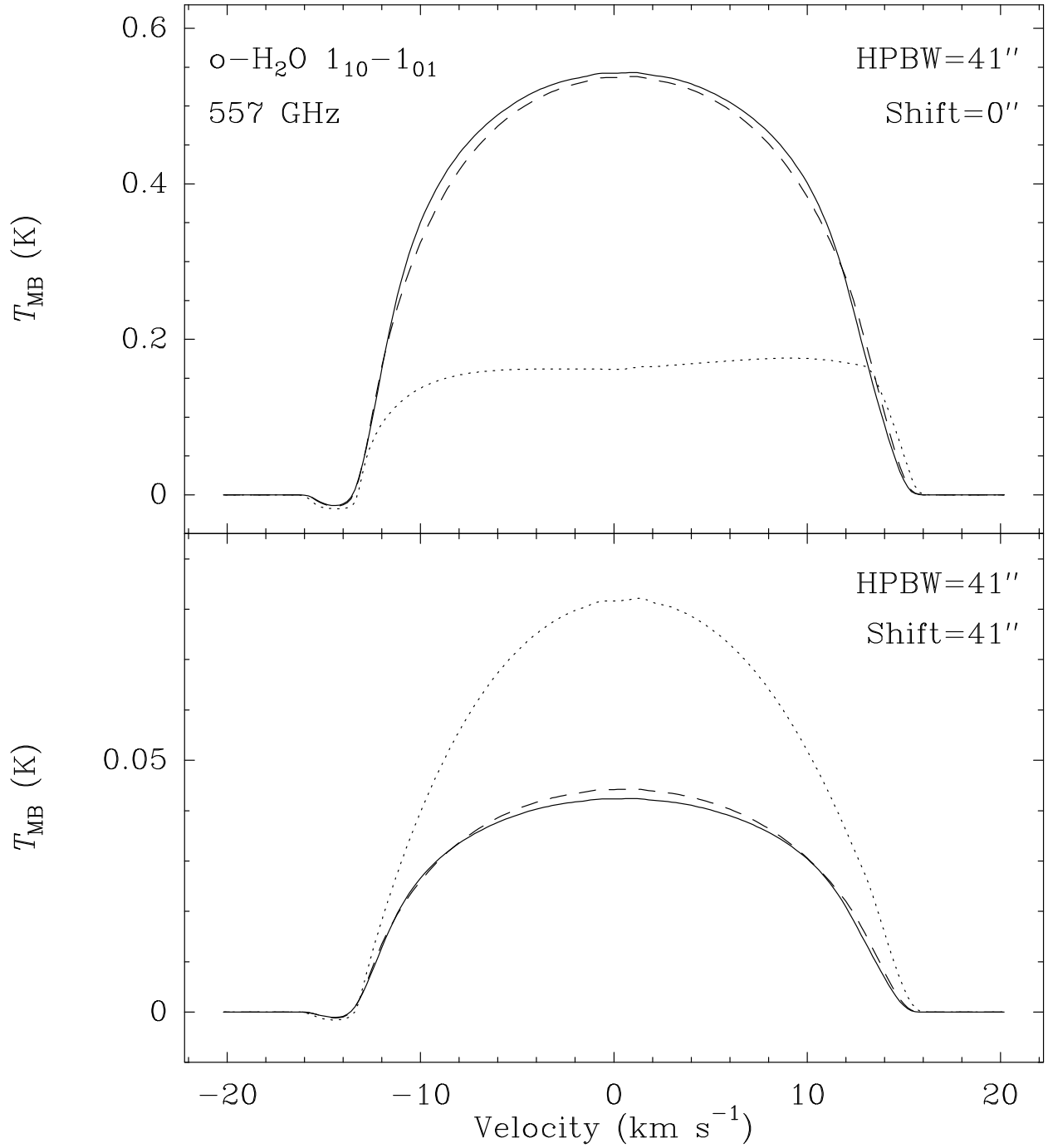


Fig. 5.— Predicted line profile of the o-H₂O $\hat{1}10101$ line with the HSO-HIFI beam, and the telescope axis pointing toward the source center (*upper*) and toward a position shifted 41'' from the source center (*lower*). Model A: solid line; B: dashed line; C: dotted line.

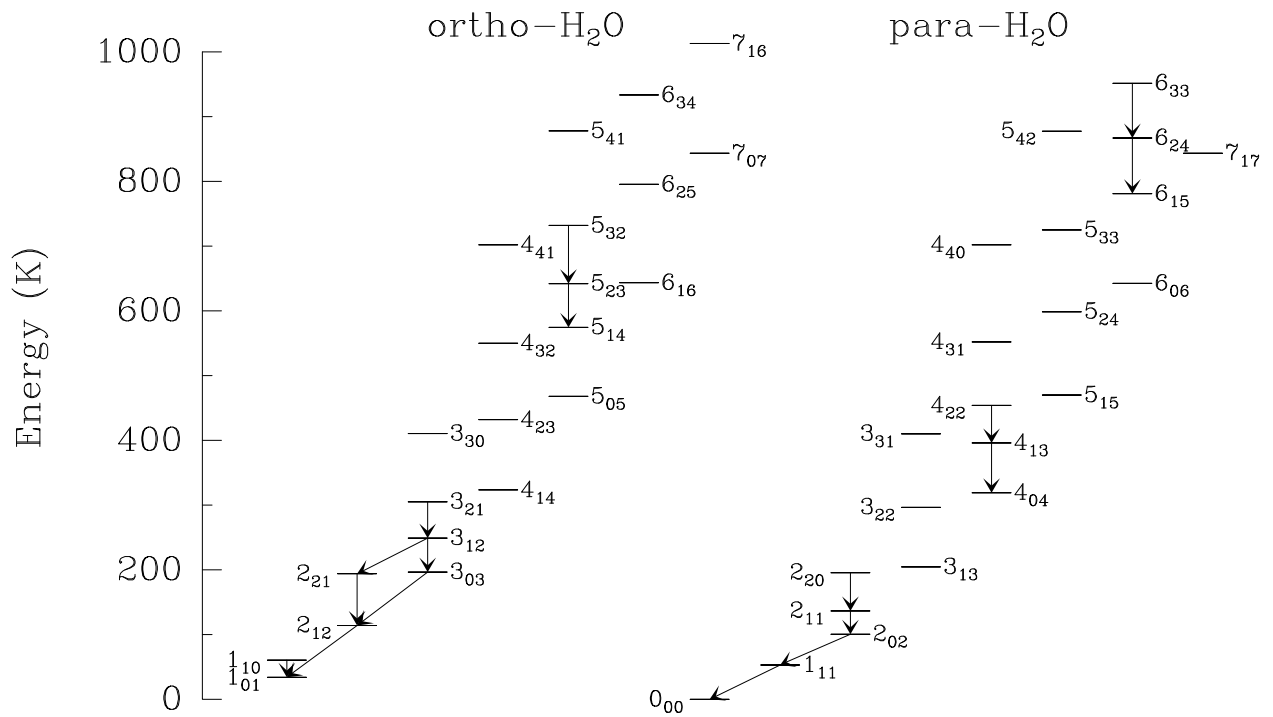


Fig. 6.— Energy level diagram of ortho and para-H₂O. Arrows indicate the transitions whose predicted line fluxes and profiles are shown in Figs. 7 and 8.

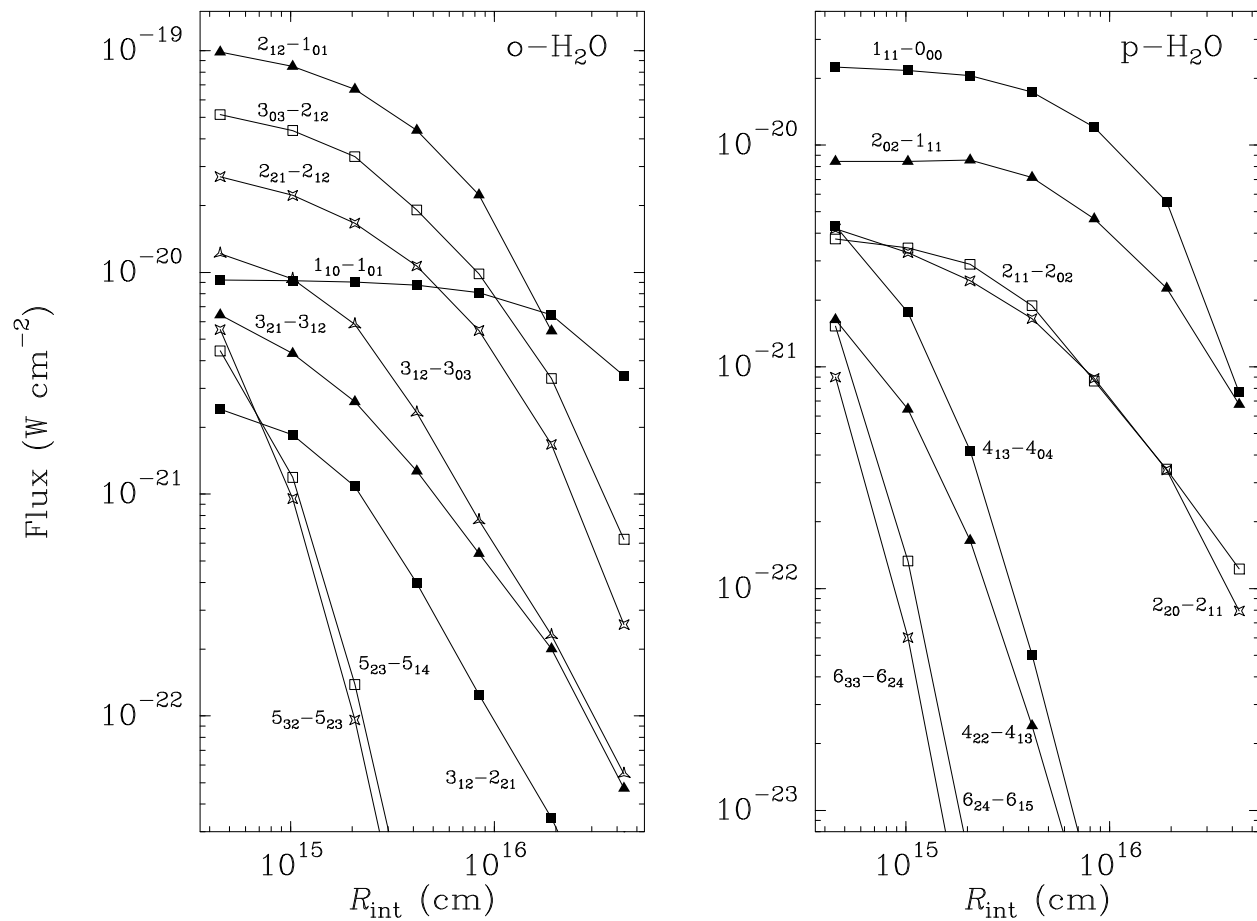


Fig. 7.— Predicted H₂O line fluxes observable by HSO-HIFI as a function of the inner radius of the H₂O shell. Adopted beamwidths are listed in Table 3.

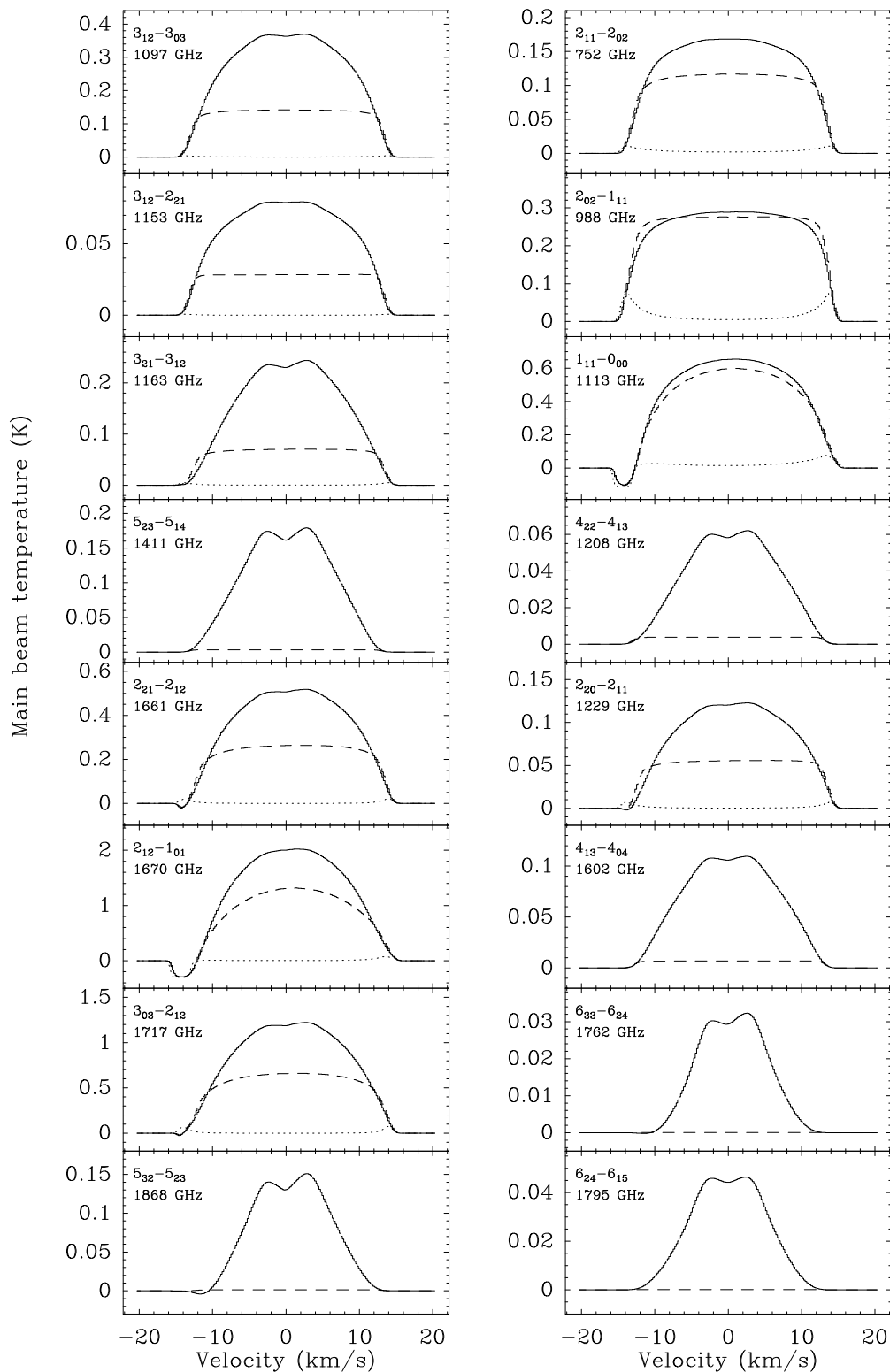


Fig. 8.— Predicted H₂O line profiles observable by HSO-HIFI, for models *A* (solid), *B* (dashed), and *C* (dotted). Adopted beamwidths are listed in Table 3.

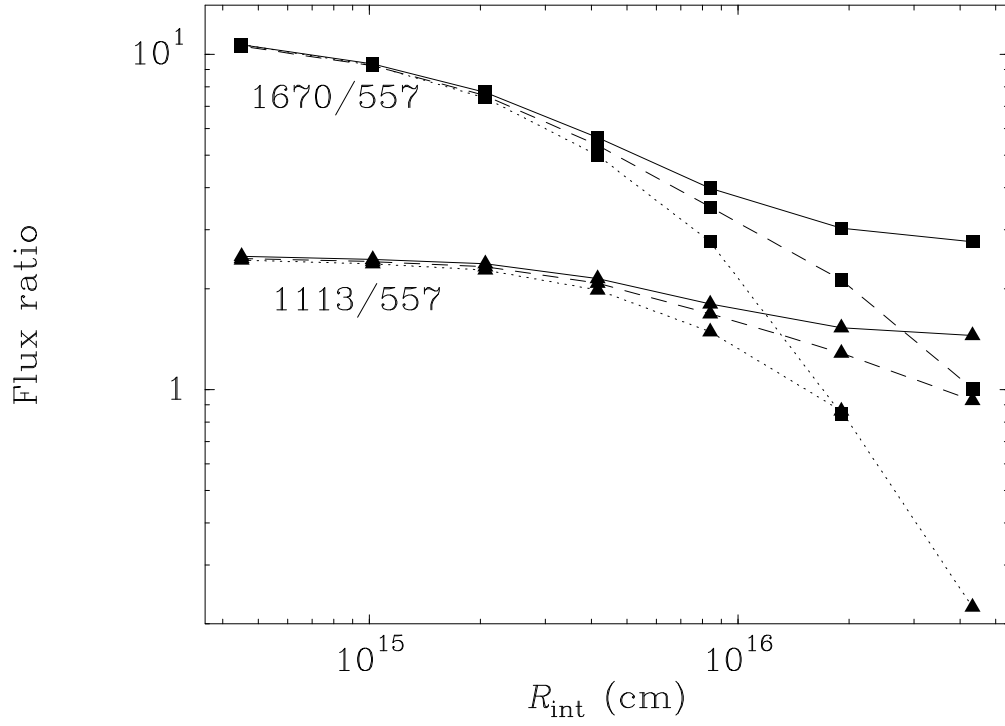


Fig. 9.— Calculated $F(\hat{2}12101)/F(\hat{1}10101)$ (labelled 1670/557, squares) and $F(\hat{1}11000)/F(\hat{1}10101)$ (labelled 1113/557, triangles) vs. R_{int} for the IRC+10216 model source, but located at a distance of $D > 2$ kpc (solid lines), $D = 0.5$ kpc (dashed lines), and $D = 0.17$ kpc (dotted lines).

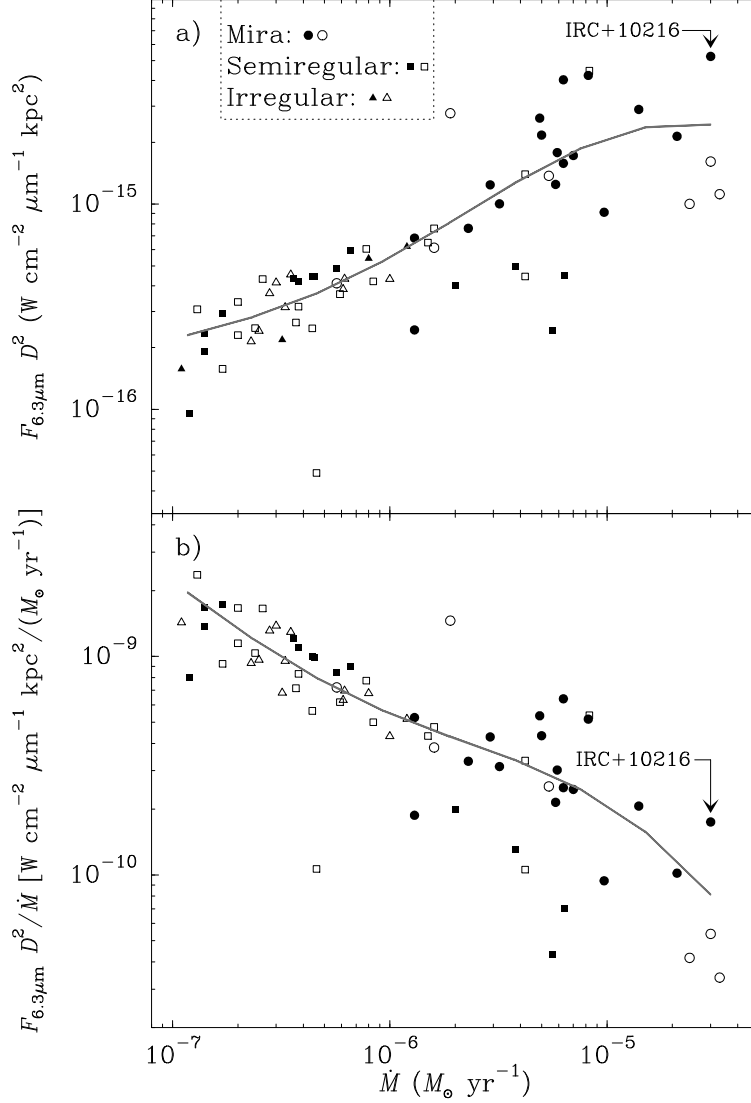


Fig. 10.— a) Continuum flux densities at $6.3 \mu\text{m}$, corrected for the distance to the sources, versus the mass loss rate for a sample of C-rich AGB stars. Filled symbols indicate sources for which the $6.3 \mu\text{m}$ flux has been directly measured from ISO/SWS spectra (Sloan et al. 2003), and opened symbols indicate sources for which the $6.3 \mu\text{m}$ flux has been estimated from the available $8.8 \mu\text{m}$ flux density (see text for details). The grey line shows the fit to the general trend achieved with our dust models. b) Same as in a) but divided by the mass loss rate. The position of IRC+10216 is indicated in both diagrams.

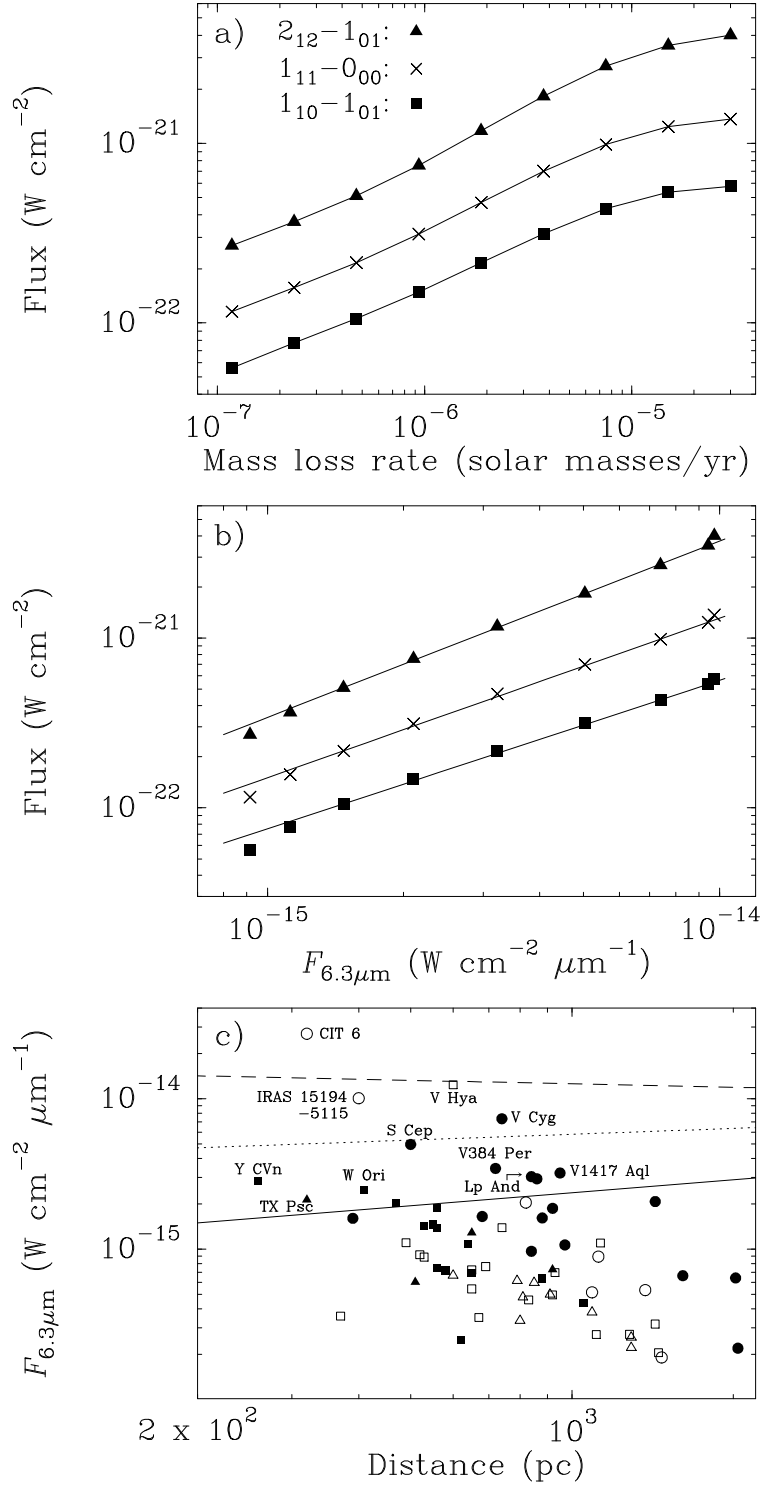


Fig. 11.— Calculated H₂O line fluxes vs. \dot{M} (a), and vs. the 6.3 μm continuum flux (b), where the lines are fits of the form $F_{\text{line}} \propto F_{6.3\mu\text{m}}^b$; results are given for a source at $D = 0.5$ kpc. c) Observed continuum fluxes at 6.3 μm of C-rich AGB stars in function of the distance (see Fig. 10 for the meaning of symbols). The lines show the 6.3 μm continuum flux required to detect the ground-state lines in 1.5 hours of observing time with HSO-HIFI, if the H₂O outflow rate is the same as that in IRC+10216 (solid: $\hat{1}_{10101}$; dotted: $\hat{1}_{11000}$; dashed: $\hat{2}_{12101}$). Some of the stars that would be detectable in such a case in the $\hat{1}_{10101}$ o-H₂O line

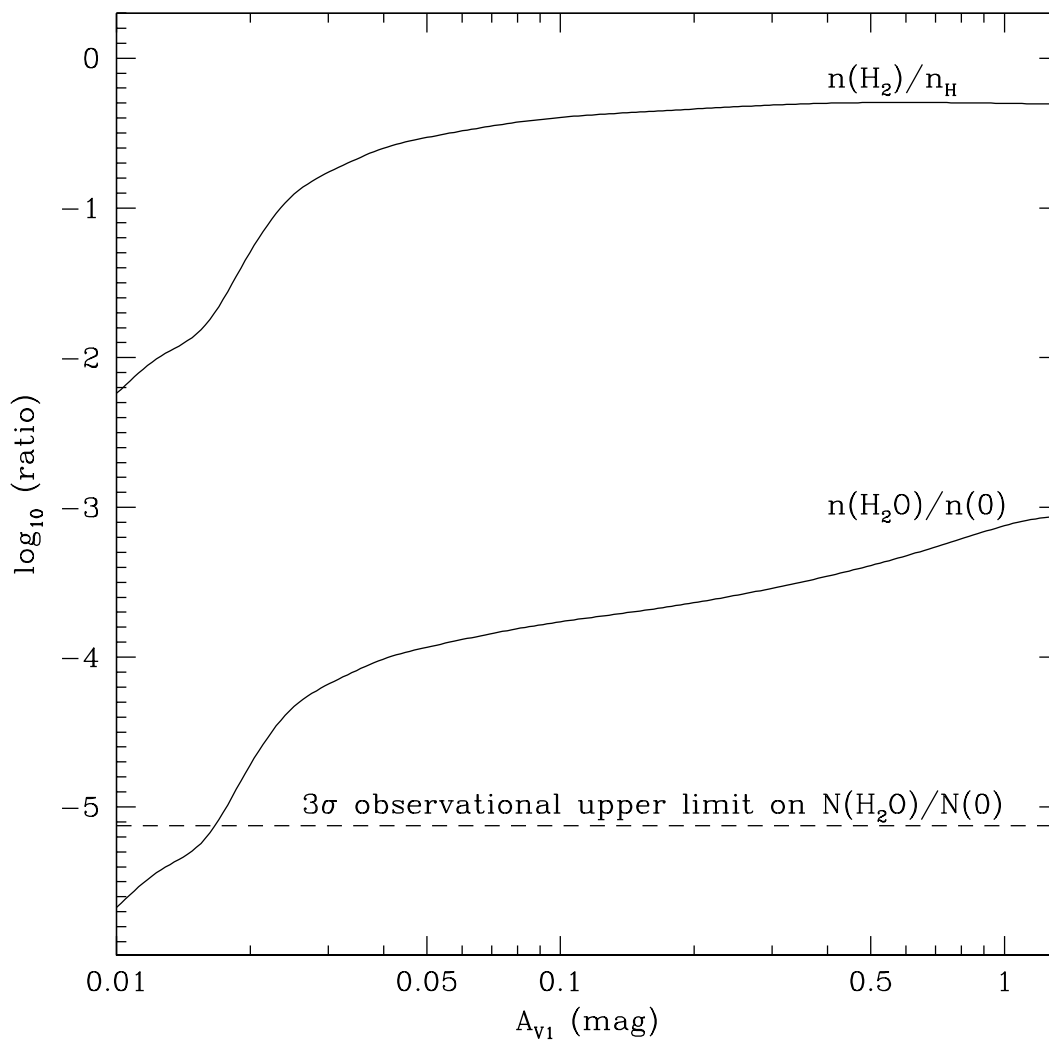


Fig. 12.— Predicted $n(\text{H}_2)/n_{\text{H}}$ ratio for the best-fit Spaans et al. (1998) model, together with the $n(\text{H}_2\text{O})/n(\text{O})$ ratio that would result if k_{ra} were $10^{-15} \text{ cm}^3 \text{ s}^{-1}$. The dashed line shows the 3σ upper limit on the observed $N(\text{H}_2\text{O})/N(\text{O})$ ratio.